chemosensors

MDPI

Review

Advances in Electrochemical Aptasensors Based on Carbon Nanomaterials

Gennady Evtugyn [1,2,*], Anna Porfireva [1], Rezeda Shamagsumova [1] and Tibor Hianik [3,*]

[1] A.M. Butlerov' Chemistry Institute, Kazan Federal University, 18 Kremlevskaya Street, 420008 Kazan, Russian; Anna.Porfireva@kpfu.ru (A.P.); Rezeda.Shamagsumova@kpfu.ru (R.S.)

[2] Analytical Chemistry Department of Chemical Technology Institute, Ural Federal University, 19 Mira Street, 620002 Ekaterinburg, Russian

[3] Department of Nuclear Physics and Biophysics, Comenius University, Mlynska dolina F1, 842 48 Bratislava, Slovakia

* Correspondence: Gennady.Evtugyn@kpfu.ru (G.E.); Tibor.Hianik@fmph.uniba.sk (T.H.); Tel.: +7-843-233-7491 (G.E.); +421-2-6029-5683 (T.H.)

Received: 7 September 2020; Accepted: 6 October 2020; Published: 8 October 2020

Abstract: Carbon nanomaterials offer unique opportunities for the assembling of electrochemical aptasensors due to their high electroconductivity, redox activity, compatibility with biochemical receptors and broad possibilities of functionalization and combination with other auxiliary reagents. In this review, the progress in the development of electrochemical aptasensors based on carbon nanomaterials in 2016–2020 is considered with particular emphasis on the role of carbon materials in aptamer immobilization and signal generation. The synthesis and properties of carbon nanotubes, graphene materials, carbon nitride, carbon black particles and fullerene are described and their implementation in the electrochemical biosensors are summarized. Examples of electrochemical aptasensors are classified in accordance with the content of the surface layer and signal measurement mode. In conclusion, the drawbacks and future prospects of carbon nanomaterials' application in electrochemical aptasensors are briefly discussed.

Keywords: electrochemical aptasensor; sensor; carbon nanotubes; graphene; carbon nitride; carbon black

1. Introduction

There is growing interest in the development of fast and reliable sensor devices intended for the determination of various species demanded in medicine [1], food quality [2] and environmental contamination monitoring [3]. The necessity in the sensors is due to many of their functions influencing health and life quality of population, e.g., early diagnostics of various diseases [4], chemical contamination detection [3,5] and better control of the agriculture production and foodstuffs [6–8]. The importance of the sensors in medicine is confirmed by impressive progress in point-of-care diagnostic devices [9–11] and lab-on-chip platforms [12–14] that combine the steps of sampling, sample treatment, separation and analysis. The continuous extension of the number of species to be analyzed in air, water and soil and the decrease in their limited threshold concentrations straighten the requirements of selectivity and sensitivity of the sensor-based analysis that exceed those formulated for conventional routine analytical instrumentation. In the last decade, many sensors have been successfully introduced into everyday life. Their application accelerated decision making in many areas sensitive to the information on the chemical content of the environment. Nevertheless, the number of chemicals under routine chemical monitoring remains quite narrow. This is due to various reasons, including the unsatisfactory analytical performance of portable analytical equipment, their insufficient mobility, and necessity in time and labor-consuming sample treatment, etc. In many cases, conventional

universal methods such as chromatography and spectroscopy have an advantage due to the possibility of simultaneous determination of many analytes, whereas sensor-based analogs are either less selective or intended for the determination of individual substances.

From the potential drawbacks limiting the further progress of chemical sensors, the problems of selectivity and molecular recognition of the analytes are considered as most important. The use of biochemical receptors, i.e., enzymes, antibodies and nucleic acids, revolutionized the area of sensor analysis, especially in medicine and life sciences. Appropriate analytical devices with biochemical components closely attached to the transducer and involved in the signal generation due to specific interaction with an analyte were named *biosensors* [15]. Since the first article devoted to glucose monitoring in blood serum, which was published in 1962 [16], biosensors have been dramatically extended toward application and now are dominate in clinical analysis of metabolites [17–19], drug discovery [20] and pathogen diagnostics [21–23]. Among many others, continuous metabolite determination [24,25], DNA-based diagnostics of pathogenic bacteria and viruses [26–28] and immunoassay [29] should be mentioned as examples of biosensor success.

The directions of the further biosensor design and areas of their application involve the introduction of new recognition elements that are responsible for specific binding of analyte molecules. Another important direction of modern investigations assumes improvement of the conditions on the biosensor interface that result in the conversion of the target biochemical interactions into the changes of chemical or physical properties recorded then as a biosensor signal. Regarding new biochemical components, DNA-derived oligonucleotides should be mentioned [30]. These substances are considered an alternative to native antibodies but show higher thermal stability, easier modification capabilities and rather simple tuning of the structure to the specific analyte molecules [31]. Started in 1990 [32–34], the application of such oligonucleotides called aptamers (from Latin *aptus* (to fit) and Greek *meros* (part)) in biosensor assembly has been dramatically increased. Presently, the number of individual compounds determined with this kind of biosensors called aptasensor become about a hundred. However, as for other biosensors, aptasensors can fully embody the advantages of aptamers only in case of the adequate arrangement of the interface with effective interconnections between the transducer, aptamer as a recognition element and the microenvironment as a source of the analyte molecules and auxiliary agents required for their binding. The selection of aptamers as well as their proper incorporation in the surface layer of the aptasensors are both indispensable parts of the aptasensor design.

This is especially true for electrochemical devices based on achievements of modern electroanalysis. The signal recorded in them with transducer mostly represented by an electrode made of conducting material is related to the redox conversion of an analyte or specific molecules added to the sample tested (redo indicators) or introduced in the structure of biochemical components (redox labels) [35]. The electrochemical biosensors dominated in the market of mobile analytical devices, among others, due to simple design, compatibility with commercial instrumentation (voltammographs, oximeters, pH-meters etc.), the well-elaborated theory of electrode reactions and the high sensitivity of the response. Although optical biosensors and especially fluorescent sensors have become privileged in current applications such as microfluidics [36], electrochemical sensors remain cheaper, simpler and easier in operation. For them, the signal and its sensitivity to the analyte tremendously depend on the electric contact on the biointerface. All the aptamers are non-conductive and hence make the electric wiring of the aptasensor worse. Besides, direct attachment of aptamers on the electrode surface is unsatisfactory due to the limited quantities of the aptamer molecules to be attached, difficulties in the formation of regular layers with predictable and reproducible thickness and the accessibility of the analytes.

Nanomaterials consisting of conductive or semi-conductive materials are the best candidates for the solution of the above problems [37–39]. This might be obvious for metal nanoparticles that offer electrocatalytic properties and amplified recorded currents. Howeverr, carbonaceous nanomaterials show many other advantages that make them very attractive in the assembly of electrochemical aptasensors. Most of them exert electroconductivity sufficient for the electric wiring of redox active

species involved in target interactions. This is particularly important for aptamers that do not exert any redox activity and need specific labels or redox indicators for signal generation. Then, many of the carbon nanomaterials contain surface groups that might be involved in the immobilization of aptamers (hydroxyl and carboxylate groups). Moreover, such groups are obtained spontaneously in mechanical treatment of appropriate materials. However, their quantities can be increased by additional chemical or electrochemical oxidation. Then, carbon nanomaterials increase the specific surface of the electrode and hence density of biorecognition elements to be immobilized. Finally, carbon nanomaterials can be easily modified by chemical treatment so that their properties, including charge, shape and size, can be directly varied in a broad range.

Recently, many reviews summarizing the achievements in electrochemical aptasensors design have been published. In them, the analytical performance of aptasensors based on nanomaterials was classified mainly in accordance with analyte nature and/or biochemical action [40–43]. In this review, the progress in the development of aptasensors based on carbon nanomaterials is presented for the last five years with particular emphasis to the role of carbon nanomaterials and mechanism of signal generation.

2. Carbon Nanomaterials

Nanomaterials involve the materials with the size in any dimension ranging from 1 to 100 nm [44]. The interest and broad application they attract result from unique thermal, mechanical, electric and biological properties not found in macro-sized analogs and other conventional materials. Some of these unique properties are related to a high surface-to-volume ratio and significant surface energy excess. Then, nanomaterials are able to form various bonds based on π–stacking, dispersion forces, dative bonds, hydrogen bonds and hydrophobic interactions [45]. The reactions highly depend not only on the size and nature of nanoparticles bot also on their orientation on the electrode interface, association and compatibility with supporting materials and pore-forming components. These features offer broad opportunities for tuning properties of the sensors modified with such nanomaterials and for adapting the signal generation conditions to both analyte and sample matrix.

Being introduced in the sensor assembly, nanomaterials can highly increase the signal and improve recognition properties toward analytes able to specifically interact with them. Besides, deposition of nanomaterials could increase specific surface area and quantity of the receptors, both artificial and natural, attached to the surface. In the case of electrochemical sensors, nanomaterials improve the conditions of the electron exchange on the electrode interface and exert in some cases electrocatalytic properties in common reactions such as oxygen reduction [46], methanol oxidation [47] or hydrogen evolution [48].

Graphene and related materials. Graphene is a single layer of sp^2 hybridized carbon atoms bonded in a honeycomb lattice [49]. Graphene is a structural unit of graphite. Since the first isolation in 2004 [50], graphene has become very popular due to its thermal, optical, electric and mechanical properties. Theoretically, graphene exhibits a specific surface area of 2630 m^2/g, two times higher than that of carbon nanotube [51]. Graphene can be produced by micromechanical cleaving, graphite exfoliation, chemical vapor deposition (CVD) [52] and organic synthesis [53]. Micromechanical cleaving ("scotch tape method") is the best in producing graphene sheets almost free of defects. However, it showed limited control on the number of peeled-off layers and is unsuitable for the mass production of graphene. In chemical vapor deposition, graphene layers are grown on single crystal supporting materials at a high temperature (over 600 °C) [54]. Solution phase exfoliation of graphite has become most popular in chemical sensors applications due to simple and predictable results of the synthesis. In this method, graphite is first oxidized in a strongly acidic environment to form graphene oxide (GO), which is then reduced by thermal, chemical or electrochemical treatments [55,56]. Unfortunately, there were not any reported applications of several types of graphene materials in a single aptasensor.

GO contains a number of the oxygen-containing functions, e.g., epoxide rings, hydroxyl, carbonyl and carboxylic groups. GO retains a single-layer structure, but it is much less conductive than graphene.

The reduction of GO results in the partial recovery of polyaromatic system and conductivity, but the product of such a treatment differs from ideal graphene by a significant number of defects and functional groups retained in its structure. For this reason, this product is commonly named as reduced graphene oxide (rGO). The structures of graphene, GO and rGO are outlined in Figure 1.

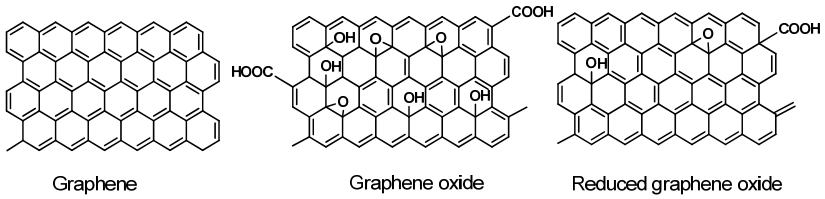

Figure 1. Idealized structures of graphene, graphene oxide (GO) and reduced graphene oxide (rGO).

Surprisingly, it has been found that rGO is more suitable than "pure" graphene in the assembly of aptasensors due to higher hydrophilicity and easier attachment of functional groups required for the covalent immobilization of the aptamers or for binding to the transducer/support surface. rGO has found numerous applications in electrochemical sensors and biosensors. In some cases [57–60], rGO particles are used as labels or redox indicators. Due to its size and flat aromatic structure, such labels act as carriers for Au nanoparticles and small redox active molecules. The examples of such application of graphene are given below. This results in amplification of the signal because one analyte molecule bonded follows the attachment of a multiply higher number of redox indicators. Meanwhile, the electroconductivity of the rGO particle ions is mostly sufficient for the electric wiring of the species involved in redox conversion on the electrode interface, including redox centers of oxidoreductases and DNA molecules.

The insertion of heteroatoms in the graphene structure (doping) is another way to regulate the defects and hence electrocatalytic activity of graphene. Thus, fluorine, boron, phosphorus and nitrogen have been introduced by a number of methods including calcination [61], liquid-phase reaction [62], CVD [63] and electrochemical treatment [64]. Such doped graphene materials have found application in the supercapacitors, batteries and photovoltaic devices but some examples of their use in aptasensors assembly exist and will be discussed later on. In addition, graphene is easily combined with inorganic and metallic composites that can be adjusted by the selection of the components choice and ratio to reach maximal synergetic effect, mechanical and chemical stability and compatibility with both the support and biochemical components of biosensors [65].

Carbon nanotubes (CNTs) are rolled up cylinders of graphene sheets. The CNTs can contain one tube (single-walled carbon nanotubes, SWCNTs) and several concentric tubes (multiwalled carbon nanotubes, MWCNTs) separated by 0.34 nm [66]. The diameter of the SWCNTs is commonly 0.4–2 nm and that of MWCNTs is 2–100 nm, depending on the synthesis conditions [67]. As synthesized, CNTs are capped with fullerene-like hemispheres from both ends. In the following oxidation normally used prior to CNT application in the sensor assembly, these caps are removed and the tubes become shorter. SWNTs show the surface area up to 1600 m^2/g [68]. As-produced MWNTs give the surface area between 200 and 400 m^2/g. Chemical treatment with KOH increases this value to about 1000 m^2/g [69].

CNTs are synthesized by arc discharge, laser ablation, and CVD. In arc discharge, carbon atoms are sublimated from solid precursors at 4000–6000 K [70]. This method does not require metallic catalysts, whose residues can alter the MWNTs' properties. In laser ablation, laser pulses ablate carbon target heated to 1200 °C. In laser plume, the temperature can reach 4000 K [71]. Both methods produce the CNTs with minimal defects on the sidewalls of the nanotubes. Amorphous carbon and graphitic particles are removed by controlled oxidation. In CVD, ethylene, acetylene or carbon monooxide is heated and passed through the tube furnace with metal catalyst at 550–700 °C. Carbon atoms are precipitated on the catalyst particles to form tubular carbon solids in sp^2 structure. Thus, commercially available HiPCO nanotubes are obtained with high-pressure CVD with Ni catalyst and CO as a carbon source.

Comparing with flat graphene, π-electron clouds in SWNTs exhibit significant curvature that results in partial σ-π hybridization. The C–C bond length is elongated from 1.41 Å (graphene) to 1.44 Å. Curvature leads to the dependence of electric conductivity and reactivity of the CNTs on their diameter and chirality expressed by the chirality angle (θ). It can be defined as a function of a pair of integers (n, m), $\theta = \tan^{-1}[3^{1/2}m/(m + 2n)]$. Here, the pair ($n$, m) ascribes the number of lattice units in the repeating part of a graphene sheet in the SWCNT [72]. SWNTs can exert metallic ($n = m$), semi-metallic ($n - m = 3k$, where k is an integer) or semi-conducting properties ($n - m \neq 3k$). For commonly used names of the SWNTs geometry, zigzag is characterized by θ = 0° and armchair configuration with θ = 30° (Figure 2).

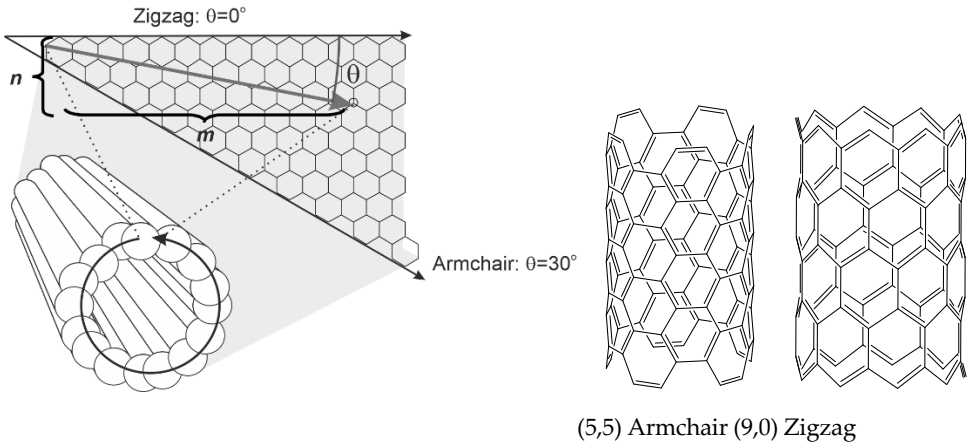

Figure 2. Outline of the single-walled carbon nanotube (SWCNT) tubes (armchair and zigzag configurations) and explanation of the chirality angle.

MWCNTs exhibit a wide diversity of the structure, which is highly affected by defects of graphene rolls. Considering relative position of inner layers, several morphological variations can be counted like hollow tube, bamboo-like MWCNTs and herringbone nanotubes. In them, graphene sheets are placed parallel to the main axis (hollow tube) or offset at a slight angle to the axis (herringbone). Bamboo-like MWCNTs are similar to herringbone structure, but inert tubes are periodically closed off into compartments like in the bamboo plant. The defects of the MWCNTs walls are decorated with oxygen-containing functional groups involved in redox catalysis of the electron transfer [73,74].

Graphitic carbon nitride g-C_3N_4 (Figure 3) is obtained by the polymerization of nitrogen rich precursors (cyanamide, urea, thiourea, melamine) performed by physical vapor deposition, CVD, solvothermal method or solid-state reaction [75]. The above reactions result in the formation of a non-volatile product, which can be transferred into the various nano- and microstructures, including nano flacks and microrods by exfoliation conducted under partial oxidation, sonication or chemical treatment. One of the common isothermal methods involves treatment of the g-C_3N_4 monolith in the nitrogen atmosphere with chloride salts (the so-called isothermal method [76]). As a result, negatively charged particles well dispersed in aqueous solutions are obtained. Dispersed products were also obtained by a cathodic reduction of carbon nitride [77]. Similar to the graphene, the *g*-C_3N_4 crystal structure can be ascribed as a hexagonal framework of the sp^2 hybridized carbon and nitrogen atoms. Two structural isomers of g-C_3N_4 exist, i.e., one derived from *s*-1,3,5-triazine core and another one from *s*-heptazine (1,3,4,6,7,9,9b-heptaazaphenalene). Appropriate subunits are connected with planar tertiary amino groups. The g-C_3N_4 exhibits semiconducting properties and the band gap (2.7 eV) makes it suitable for photocatalytic and electrochemiluminescence (ECL) processes [78,79].

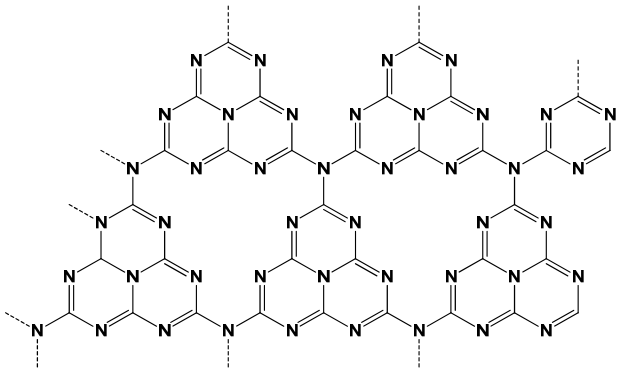

g-C_3N_4 on *s*-heptazine core

Figure 3. Idealized structure of graphitized carbon nitride (g-C_3N_4).

Carbon black (CB) is mostly obtained by combustion of petroleum products They consist of the spherical nanoparticles with a diameter from 3 to 100 nm, which are often bonded to each other to form aggregates. The CB surface area can vary from 15 to 1000 m^2/g, and the electroconductivity ((1.0–2) × 10^3 Sm^{-1} [80]) is higher than that of CNTs (0.02–0.25 Sm^{-1} [81]). The CB nanoparticles have a high concentration of oxygen-containing surface groups that can be involved in the covalent attachment of many biochemical receptors. Together with low cost and high accessibility, these properties make CBs very attractive for use in voltammetric biosensors [82]. Some other materials obtained in a similar manner should also be mentioned. These materials include acetylene black, which is formed in acetylene combustion and is applied in the modification of electrodes as transducers of the DNA [83] and enzyme [84] biosensors.

Fullerenes are allotropic modifications of the carbon in the form of symmetrical clusters. In them, carbon atoms in the sp^2 hybridization state are bonded to each other on the surface of a sphere at the vertices of pentagons and hexagons [85]. C_{60} fullerene is most intensively investigated (Figure 4). It consists of 20 hexagons and 12 pentagons with a diameter of 0.7 nm. Fullerenes are synthesized by electric arc discharge [86], electron beam ablation [87] and sputtering [88]. However, most of these methods cannot provide sufficient quantities of the product with a regular structure. Fullerenes are rather easily modified with many functionalized compounds via defects of the structure or intermediate formation of epoxy rings. Besides, fullerenes can interact with CNTs and graphene materials by hydrophobic interactions. Meanwhile fullerenes exert efficient electron exchange ability and can mediate electron transfer in the assembly of various electrochemical sensors and biosensors with electrocatalytic response [89,90].

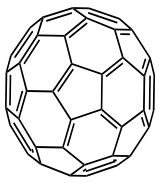

Figure 4. Idealized structure of the fullerene C60.

Carbon dots (CDs) are zero-dimension materials based on graphitic cores, which are classified in accordance with the size, structure, source and specific properties [91]. Most of them are applied in optic methods of analysis and energy storage devices. Besides CD classes, carbon nanodot, carbon quantum dot, and graphene quantum dot classes are mentioned [92–94]. Thus, in electrochemical sensors, graphene quantum dots are frequently utilized. They consist of up to ten single atom layers with obvious graphene lattice and have a lateral dimension of about 100 nm [95]. Meanwhile, such graphene quantum dots are more hydrophilic than graphene and have a higher electrocatalytic activity due to the predominant participation of edges in the electron transfer. Graphene quantum dots are

synthesized by the electrochemical [96] or ultrasonication exfoliation [97] or by pyrolysis of small organic molecules such as trisodium citrate (hydrothermal method [98]). Carbon nanodots are smaller (spherical particles of about 10 nm in diameter). They are mostly used in the electrochemical sensor assembly after functionalization with redox labels or receptors. Carbon nanodots are obtained by the methods described above for the CNTs synthesis. Among others, hydrothermal carbonization is currently considered the most suitable method due to its low cost, environment- and user-friendly protocol and possibility of mass production of the product [99]. In this method, organic precursors (proteins, glucose, citric acid, or chitosan) are heated in reactor. Nitrogen doping and the synthesis of the composites with inorganic components can be performed by addition of appropriate materials to the same solution. The additives can also serve as solid templates for the formation of porous particles with carbonic shell and compact core. Thus, the use of proteins allows for the synthesis of carbon dots containing up to 8 wt.% of nitrogen [100]. The carbonization of biomass can be effectively promoted by addition of Fe^{2+} ions [101]. Electrochemical properties of carbon nanodots and their application for electrochemical sensing have been recently reviewed in [102].

3. Aptasensor Assembly

3.1. Aptamer Immobiization

The immobilization of aptamers should provide reliable sensitive signal and its minimal drift during the aptasensor storage and operation period. Similarly, to other biosensors, all the aptamer immobilization protocols can be divided into three main groups, i.e., physical adsorption, chemical (covalent) and affinity immobilization. Their advantages and drawbacks are briefly described below. It should be noted that only methods described for assembling aptasensors based on carbon nanomaterials are mentioned and the variety of all the immobilization protocols is certainly wider.

Physical adsorption is based on weak multiple interactions involving electrostatic, donor-acceptor and hydrophobic interactions, as well as van der Waals and hydrogen bonds. The aptamers commonly bear negative charge related to the phosphate residues of the backbone and hence they can be rather easily accumulated on positively charge carriers. For this purpose, some polyelectrolytes, such as poly(ethylene imine) (PEI) [103,104], poly(diallyldimethylammonium chloride) (PDDA) or polyaniline [105], are used as a kind of molecular "glue" combining oppositely charged components of the surface layer (e.g., carboxylated carbonaceous materials and aptamers). Electrostatic assembling is governed by the charge density and flexibility of the charge carriers and is also affected by small ions present in the solution as a supporting electrolyte. As for electrochemical aptasensors, electrostatic accumulation can be improved by preliminary polarization of the electrode or its partial oxidation resulted in formation of carbonyl and carboxylate groups on the surface of electrode or the nanomaterials deposited on its surface [106]. In some cases, such oxidative treatment is performed on the preliminary stages of electrode assembling for cleaning or suspending of the carbon nanomaterials with no respect of the signal transduction. Physical adsorption is the simplest immobilization method and is performed by drop casting of the aptamer solution on the pretreated surface. Excessive quantities of reactants are removed by washing. The addition of oppositely charged polyelectrolytes can result in the formation of multilayered complexes, where the aptamer layer is additionally protected from desorption by polyelectrolyte deposited on its surface (layer-by-layer immobilization) [107]. This protocol makes it possible to vary the charge and roughness of the layer by selection of appropriate polyelectrolytes. PEI and PDDA are mostly used in these complexes as cationic species.

Physical adsorption provides reproducible characteristics of aptasensors due to self-assembling and self-organization principles. The results depend on the quality of underlying surface and immobilization conditions (ionic strength, pH, buffer composition, temperature). On the other hand, non-covalent immobilization is reversible and does not guarantee from the losses of aptamer molecules if sharp changes of the electrolyte content or of the solution pH takes place. In the case of graphene and, to a lesser extent, CNTs, hydrophobic interactions of polyaromatic lattices can be used for the

immobilization of aptamers via the π-staking of aromatic systems [108]. For this purpose, pyrene fragments are first covalently attached to the terminal groups of aptamers. Physical adsorption is compatible with microfluidic techniques and paper based electrochemical sensors.

Chemical (covalent) immobilization includes the formation of covalent bonds between the aptamer and carrier. For this purpose, terminal functional groups are introduced in the aptamer assembly. If Au or Ag nanoparticles or a bare golden electrode are used as carriers, the thiol terminal group spontaneously forms the bonds Au(Ag)-SH, providing strong binding of the aptamer to the electrode [109,110]. The primary amino group is another common modifier compatible with glutaraldehyde and carbodiimide binding. In the former case, the reaction takes place between two amino groups with the formation of the Schiff base that can be then reduced by $NaBH_4$ to a more stable amino group (Figure 5).

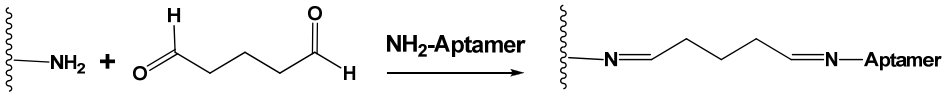

Figure 5. Glutaraldehyde cross-binding of aminated aptamer and carrier.

Chitosan or ethylene diamine can be the counterparts of glutaraldehyde binding. Excessive aldehyde groups are removed by treatment with glycine. The reaction is performed at ambient temperature with glutaraldehyde solution or vapors.

Carbodiimide binding accelerates the reaction between amino and carboxylic groups to the formation of the amide bond. Commonly, carboxylic groups are present on the surface of carbonaceous materials, and the amino group is introduced in the assembly of an aptasensor sequence. 1-Ethyl-3-(3-dimethylaminopropyl)carbodiimide (EDC) and *N*-hydroxysuccinimide (NHS) are common reactants applied for carbodiimide binding [111] (Figure 6). The protocol assumes preliminary treatment (activation) of the carrier with consecutive addition of aminated aptamer. The reaction is not complicated with oligomerization of the reagent or formation of multiple covalent bonds preventing access of an analyte.

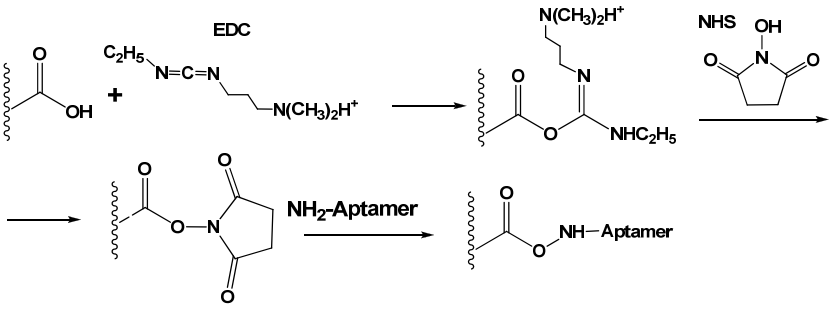

Figure 6. Principal scheme of the EDC-NHS-based carbodiimide binding of aminated aptamer to carboxylated carrier.

Introduction of carboxylate function on the electrode interface can be also performed using diazonium salt generated in situ. In this method, *p*-nitrobenzoic acid is first electrochemically reduced in acidic media to amino derivative, which is transformed into diazonium salt by sodium nitrite. The subsequent cathodic reaction results in the formation of phenylcarboxylic radicals that are attached to the surface of screen-printed electrode, CNTs or graphite paste electrode (electrografting protocol) [112,113]. Easy handling and formation of dense monolayers with reproducible predicable structure offer dense packing of the aptamers required for many protocols of the signal generation. The mechanism of generation of diazonium salt and its reaction with CNTs is outlined in Figure 7.

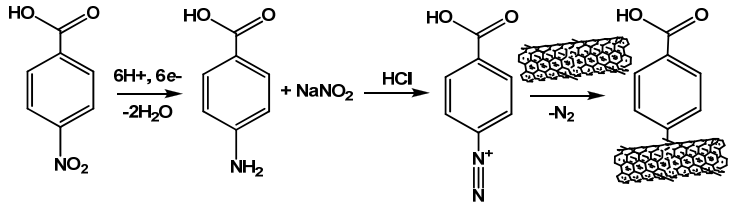

Figure 7. Principal scheme of modification of CNTs with carboxyphenyl radicals generated in situ from appropriate aromatic amine.

Contrary to physical immobilization, covalent binding is site specific and provides a certain orientation of the aptamer against the underlying surface. However, the rigidity of the binding site structure and irreversible character of the immobilization require additional measures to avoid spatial limitation of an analyte access and recognition. Thus, long-chain spacers consisting of thymidine fragments (polyT), methylene or oxyethylene units significantly decrease the steric hindrance of the analyte recognition and binding [114]. Besides, spacer selection offers new opportunities in tuning the hydrophobicity and flexibility of the spacer in accordance with the nature of the underlying layer [115].

Affinity immobilization assumes application of native receptors with a very high efficiency of recognition. The avidin (streptavidin)–biotin pair is the most popular example of such interactions. The protein part of this pair (avidin or streptavidin) can bind up to four biotin molecules. The latter ones can be easily attached to an aptamer or to another protein molecule via the carboxylic group (Figure 8).

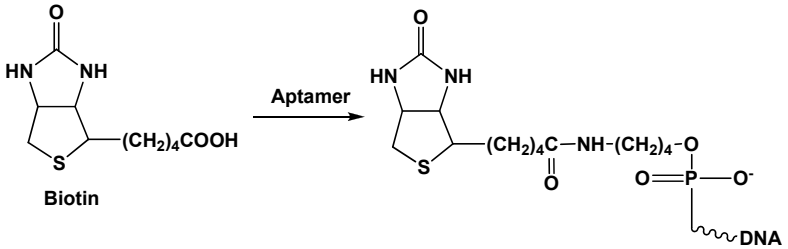

Figure 8. Modification of aptamer with biotin.

This allows for assembling branched complexes on the solid support or electrode surface and employs detection schemes similar to those of the ELISA assay or DNA hybridization analysis. Due to high affinity (dissociation constant K_D ~ 10^{-14}–10^{-15} M [116]), the avidin-biotin binding is comparable to that of antigen–antibody interaction, with higher stability to high temperature and hydrolysis.

Another affinity immobilization protocol has been proposed for label-free methods of the signal detection. In them, the auxiliary DNA sequence, complementary to the part of the aptamer (capturing DNA strand), is covalently attached to the electrode via carbodiimide binding or the Au–SH interaction described above for covalent immobilization [117,118]. The non-complementary part of aptamer can bind to an analyte. This commonly results in the folding of the linear aptamer conformation and increased density of the surface layer. Alternatively, the aptamer–analyte reaction results in the dissociation of the DNA–aptamer helix followed by the release of the aptamer–analyte complex from the electrode interface to the solution (displacement protocol). Details of signal generation in both cases are considered below in the Section 3.2.

3.2. Aptasensor Assembling

The immobilization of aptamers is of great importance for aptasensor assembling, but it is not the only step of the aptasensor assembling. In the case of using carbon nanomaterials, some additional steps are required prior to or together with the aptamer attachment.

- Synthesis or preliminary treatment of carbon nanomaterials

- Electrode cleaning and treatment
- Aptamer modification/immobilization
- Labels/indicators implementation

At present, most of the carbon nanomaterials used in the assembly of electrochemical aptasensors are commercially available. In many cases, they are already modified in a manner most convenient for their use in aptasensors design. Thus, CNTs are pre-oxidized to remove fullerene hemispheres, metal catalyst residues and amorphous carbon inclusions. Only carbon dots are still prepared by the research team that developing the aptasensor. This might be referred to a rather simple and inexpensive route of their synthesis and limited availability of appropriate products to be used as they are. The GO and related graphene materials take an intermediate position: the GO suspensions are commercially available, but their reduction is often performed or adapted within the study of aptasensors. On another hand, Hummers' method of graphite oxidation to graphite oxide and then to GO [119,120] is also applied for GO synthesis instead of commercial product use. As a result, many articles devoted to the GO and rGO in the aptasensor assembly contain very similar photographs illustrating FTIR spectra or scanning electron microscopy (SEM) images of the primary coatings that should convince reader in chemical nature and structure of 'home made' GO (rGO) particles [121–125]. If the carbon nanomaterials are intended for the increased roughness of the electrode active area and bigger quantities of aptamer immobilized, such attention to the peculiarities of the carbon particle structure seems exhausting and actually does not contribute to better understanding of the aptasensor behavior. The situation is opposite if the same nanoparticles serve as redox labels or carriers for such labels. In this case, shape, size, charge and durability of the particles, both initial and modified with aptamers and redox labels, are of critical importance for the aptasensor performance.

Electrodes applied for aptasensor assembling are presented by a glassy carbon electrode (GCE), an Au electrode and a number of screen-printed electrodes with carbon and gold as an electroconductive layer. Their preliminary treatment does not dramatically differ from that described for other biosensors and electrochemical sensors. All the manipulations are directed to the removal of impurities, the polishing of the surface and the final production of the functional groups, which are available for the following immobilization or adsorption of other components. In the case of GCE, partial oxidation with the formation of oxygen-containing functional groups takes place during mechanical polishing and can be activated by electrochemical protocols (polarization, multiple cycling in strong acids etc.). Au electrodes should be thoroughly cleaned to provide a repeatable surface for covalent attachment of thiolated species. Deposition of carbon nanomaterials as well as their combination with Au (Ag) nanoparticles chemically or electrochemically deposited onto the primary modifier correct mechanical defects of the bare electrode and make milder the requirements to its treatment. This does not mean that primary cleaning becomes exhausting because such stages predetermine the efficiency of the nanoparticles loading and holding on a flat even surface. The choice of primary electrode (GCE vs. Au etc.) depends rather on the protocol of aptamer immobilization (availability of thiolated and aminated aptamers) than on specific electrochemical reactions that commonly require low working potential and do not assume specific interactions with underlying surface.

Contrary to carbon nanomaterials, aptamers bearing specific functional groups are not synthesized but mostly ordered and bought from appropriate suppliers. In the past years, few works devoted to the optimization of the aptamer sequence toward certain analytes were published in the framework of electrochemical aptasensors design [126,127]. However, commercial aptamers should also be pre-treated depending on their structure and/or immobilization protocol. Most often, they are slowly heated and/or treated with chemical reductant for mild breaking of the internal S-S bonds and de-hybridization of random parts of their sequences. After that, they are slowly cooled to ambient temperature and drop-casted on the modifier surface, where left to react with them to for regular coating.

The inclusion of specific functions responsible for aptamer signal can be performed at any stage of the aptasensor assembling. It should be performed in a manner providing close proximity of aptamer and redox active parts of the layer. In some cases, the formation of appropriate hybrids can be

performed in one step. Thus, the formation of polymerized components can be assisted with reduction of GO [128,129].

In most cases, the formation of the layers during the loading of certain components and aptamer immobilization is monitored by conventional tools including SEM and atomic force microscopy (AFM) images, electrochemical impedance spectroscopy (EIS) and direct current (DC) cyclic voltammetry. In addition to the visualization of the surface changes with SEM and transmission electron microscopy (TEM), EIS and DC data make it possible to assess the permeability of the surface layer and the rate of the electron transfer. Ferri/ferrocyanide ions $[Fe(CN)_6]^{3-/4-}$ taken in a 1:1 molar ratio are mostly used in these experiments. This redox indicator exerts reversible behavior in electron exchange reaction, which is pH independent and does not respond on the dissolved oxygen in solution. It is important that the charge of the $[Fe(CN)_6]^{3-/4-}$ ions does not allow its accumulating on the aptamers because of the multiple phosphate anions present in their structure and bearing the same charge explaining repulsion of the indicator from the aptamer. Previously, it was established that the application of the $[Fe(CN)_6]^{3-/4-}$ redox indicator has some limitations in EIS measurements performed on Au electrodes [130]. However, no evidence of the reaction between the indicator and gold was reported within the present review area.

3.3. Signal Measurement Modes

In spite of a variety of the components implemented in the surface layer of the aptasensors, there are a limited number of signal measurement protocols, which are similar for many affinity biosensors assuming reversible binding of an analyte on the transducer surface:

- Measurement of the changes in the permeability of the surface layer using diffusionally free redox indicator.
- Monitoring signals of the redox active labels remaining attached to the electrode interface.
- Application of biochemical approaches of signal amplification based on the use of enzymes, sandwich assay and amplification of the DNA strands in the exonuclease assisted reaction cycles.

The examples of particular aptasensors using the measurement protocols mentioned will be given in the following sections devoted to the applications of carbon nanomaterials. Here, general description of the protocols is presented.

Permeability assessment. The first approach mentioned is also called the label-free detection mode. In such an approach, the transfer of the redox indicator is monitored by the current of its redox rection at the electrode. Differential pulse (DPV) or square-wave (SWV) voltammetry are used for this purpose because of their higher sensitivity against the DC mode. The principal scheme of the measurement is presented in Figure 9.

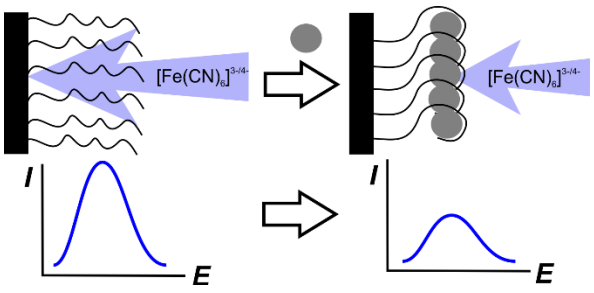

Figure 9. Principal scheme of the label-free measurement of the aptasensor signal.

It should be noted that the signal of $[Fe(CN)_6]^{3-/4-}$ redox indicator always decays after the binding of the analyte molecule. In this respect, the choice of DPV (SWV) voltammetry becomes not obvious. Indeed, the range of the changes recorded is limited by the value of the initial current obtained prior to the contact of the aptasensor with the analyte. In this case, the possibility of the decay quantification depends rather on the accuracy of the peak current detection than on the value of this signal. Assuming

that the common deviation of the above value typical for a solid-state electrochemical sensor is equal to 2%, this gives a resolution of the possible measurements of 50 independent values (100%/2%) with no respect to the concentrations varied. Nevertheless, the approach to the use of the most sensitive techniques (DPV and SWV) dominates and in many publications preliminary study on the conditions for the signal measurement are performed with cyclic voltammetry (DC mode), allowing for much better visualization of the results but the calibration graph is obtained using PDV or SWV modes.

The decrease in the current unambiguously reflects the binding of an analyte to the aptamer attached via terminal functional group to the electrode surface. two mechanisms of such influence are considered, i.e., (i) decrease in the diffusion rate caused by the implementation of additional non-conductive agent (analyte molecules) in the surface layer and (ii) increased electrostatic repulsion between the anionic redox indicator and negatively charged phosphate groups of the aptamer sequence. Although most of the analytes determined with aptasensors belong to small molecules, their influence on the permeability of the surface layer is increased to the changes in the conformation of the aptamer sequence. Thus, guanine-rich fragments of the aptamer molecule can reversibly fold to so called G4 quadruplex (Figure 10) that significantly increases density of the surface layer and its charge [131,132]. G4 quadruplexes are stabilized by central cation (normally, K^+). For this reason, electrochemical aptasensors are often sensitive to the electrolyte composition and namely potassium content [133].

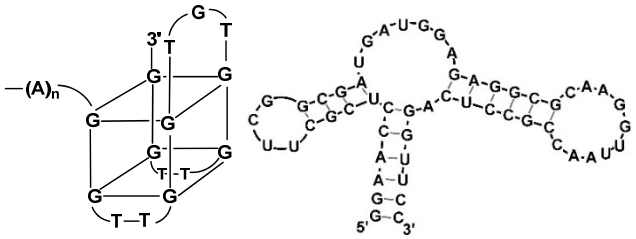

Figure 10. Examples of G4-guadruplex formed in the guanine-rich part of the aptamer molecule and pinhole aptamer.

Pinhole aptamers with pseudo-circle areas subdivided with self-hybridized double-stranded items are another example of the aptamers, dramatically changing their conformation in an analyte recognition. Being synthesized for the so-called E-sensors [134], they contain two terminal groups applied for attaching to the electrode and for the binding label to be detected. Transfer from pinhole to linear structure increases the distance between the label and electrode as decreases the signal (Figure 11).

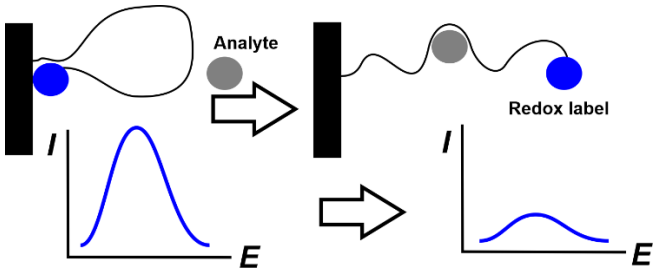

Figure 11. Detection of the signal with E-sensor based on labeled pinhole aptamer.

Methylene blue and ferrocene are mostly used in such aptamers. Although their application in combination with carbon nanomaterials is rather rare, such an approach offers opportunities in creating label- and reagent-free aptasensors with one-step measurement protocol.

Both mechanisms affect charge transfer resistance measured by EIS in the presence of the same redox indicator. Measurement is performed at the equilibrium potential assessed as a half sum of the peak potentials on a cyclic voltammogram of the $[Fe(CN)_6]^{3-/4-}$ redox pair. Its shift with the deposition

of the layer components is interpreted in terms of the charge and electroconductivity of the compounds deposited. The sensitivity of the EIS measurement is commonly higher than that of voltammetry but the choice of equivalent circuit for data fitting and EIS parameters calculation can be a source of possible errors and false conclusions. This is especially true if the interface of the aptamer–analyte interaction is far from the plane assumed in most common Randles circuit applied. The higher the roughness is the more complicated is the circuit and the more parameters are introduced to meet real behavior of an aptasensor.

Assessment of the permeability of the aptasensor layer and its changes with analyte concentration offer strict requirements to the morphology of the aptamer layer. Ideally, monolayer with regular structure and no defects with naked electrode "holes" is desirable. The use of golden bare electrode including EIS and surface plasmon resonance (SPR) measurements are near this ideal. In the case of the deposition of carbon nanomaterials and for other primary transducers applied, the interface is additionally treated with the substances preventing the non-specific adsorption of reactants and analyte is necessary. Bovine serum albumin for GCE and thiolated alcohols for the Au electrode are mentioned at this stage of aptasensor assembling [135–140].

The detection of label signals or redox indicators remained in the aptasensor surface layer. Although permeability assessment is a general approach popular for all the affinity biosensors, including those based on immunoreactions and single-stranded DNA probes, it leaves occasions for false decisions due to non-specific adsorption and possible defects in the surface layer. This might be crucial, especially in real sample analysis. Alternative approaches to the signal measurement utilize more specific substances. The use of covalently attached labels and redox probes specifically interacting with DNA/aptamer molecules is one of such solutions becoming popular in the past decade. Ferrocene and Methylene blue are mostly applied as such redox active substances. They can be covalently attached to the aptamer sequence like in the case of E-sensor described above [134]. Meanwhile, Methylene blue is often used in the soluble form due to its ability to interact with single- and double-stranded DNAs with appropriate changes of its redox activity. Possible protocols combine the concept of E-sensor with pinhole aptamer and displacement mode that is often used in affinity biosensors. The reaction schemes are outlined in Figure 12.

In these aptasensor, auxiliary single-stranded DNA (capturing DNA) is used to attach the aptamer to the electrode surface by a hybridization step. The double-stranded product of hybridization is saturated with Methylene blue molecules, which can both intercalate the DNA helix and adsorb in the minor grooves on the DNA surface. Its signal is not as high because of the shielding of the molecules intercalated DNA. After the addition of the analyte molecules, the formation of aptamer–analyte complex shifts the hybridization equilibrium and liberates auxiliary DNA remaining attached to the electrode. After the removal of all dissolved components, the Methylene blue signal decreases against its primary value because of the partial leaching of dye molecules from the surface layer and their substitution with the analyte molecules (Figure 12A). In the second protocol, auxiliary DNA with terminal redox label contains complementary fragments capable of self-hybridization and the formation of pinhole configuration. However, its reaction with complementary aptamer prevents this conformation and the redox label is placed too far from the electrode for a fast electron transfer. The removal of the aptamer binding to analyte molecules restores the pseudo-circle configuration of the auxiliary DNA and makes the label positioned in the proximity of the electrode surface (Figure 12B). In the second case, ferrocene label is used together with Methylene blue.

Aptamer can also be modified with redox label. In this case, it first attaches to the electrode surface by hybridization with a partially complementary DNA strand (capturing DNA) and then released in the solution in the complex with an analyte (Figure 12C).

Signal amplification strategies. Although carbon nanomaterials increase the signal due to the enhancement of the surface area for aptamer immobilization and due to the multiplication of the redox labels covalently attached to their surface, an additional increase in sensitivity can be reached by the implementation of catalytic cycles based on electro- or enzymatic catalysis or biochemical approaches

to the DNA amplification. Enzymes as labels in aptasensors employ the strategy well known in ELISA and sandwich immunoassay [141,142]. Here, peroxidase and its natural (hemin) and artificial analogs (Pt catalysts, metal-organic framework particles) are introduced in the aptamer–analyte complex and then monitored by the catalytic current related to H_2O_2 reduction/oxidation. The similarity is stressed by the possibility of joining both approaches and assemble a hybrid complex on the surface with aptamer attached to the electrode and secondary (signaling) antibody to the analyte molecule. Enzyme is then immobilized onto the hybrid complex by avidin-biotin binding [143].

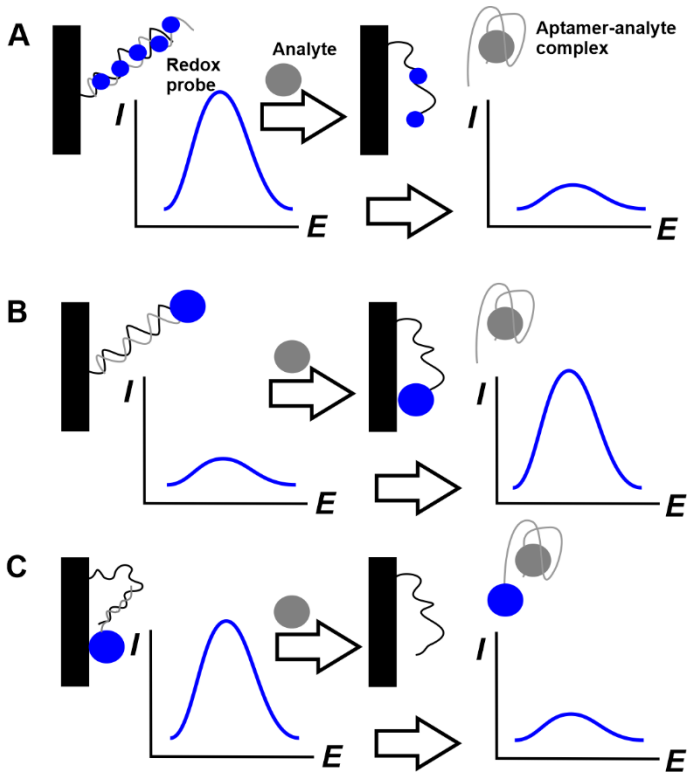

Figure 12. Schematic outline of the aptasensor with a free (A) and covalently attached (B,C) redox probe.

With regard to the amplification of the DNA quantities at the electrode interface, such approaches offer superior sensitivity and selectivity with the limit of detections (LOD) on atto- and femtomolar levels. In them, auxiliary DNA strands are involved in the polymerization cycle with formation of a long DNA sequences consisting of partially complementary strands, those formation assisted with exonuclease is triggered by target recognition of an analyte molecule. First developed for fluorescence detection [144], such systems are rather complex and rarely use carbon nanomaterials due to requirements of site-specific immobilization and careful arrangement of all the reactants on the transducer interface. In addition, some reactions are performed in bulk solution so that this protocol is not exactly a biosensor but biosensing device.

In another example, Y-DNA, containing three strands partially complementary to each other, was applied for assembling the G4 quadruples/hemin complex from two pinhole aptamers and another one immobilized on the electrode surface. The catalytic cycle of the analyte release resulted in the amplification of the quantities of the complex mimicking peroxidase activity in the presence of hydrogen peroxide. This improved the electrochemical performance of the biosensor due to the oxidation of Fe(II) in hemin [145].

Other detection schemes. The above description does not exhaust the variety of the methods for monitoring aptamer–analyte interactions described in the aptasensors using carbon nanomaterials. Thus, the intrinsic redox activity of electroactive polymers such as polyaniline and polypyrrole changes with analyte binding due to variation of the charge distribution and counter ion access within the

polymer layer [105]. In some cases, aptamer acts as a specific sorbent and accumulates analyte molecules for their following oxidation on electrode. Although such approaches show lower sensitivity against main schemes described above, they offer reliable results due to control of the processes on the electrode by working potential and its shift with the analyte addition. Then, doped MCNTs and graphene nanosheets have been described in the assembly of field effect transistors (FET) [146–148]. Appropriate aptamers can be immobilized on their surface by hydrophobic interactions. In such devices, aptamer folding caused by target interaction results in significant changes of the charge near the gate area of the FET and hence the currents flow between source and drain. This can find analytical applications though the range of concentrations determined could be rather narrow.

4. Carbon Nanomaterials in the Assembly of Electrochemical Aptasensors

4.1. Carbon Nanotubes

The analytical performance of electrochemical aptasensors with the CNTs in their assembly is summarized in Table 1 for last five years (2016–2020). Some other examples of application of the CNTs in combination with other carbonaceous nanomaterials are considered below in the sections devoted to the second component of the mixture (graphene or g-C_3N_4).

As mentioned above, CNTs play a rather passive role in the assembly of electrochemical aptasensors. Though they can exert electrocatalytic activity, which is attributed to the edges of the graphene rolls and sidewall defects; it is rarely used for signal amplification. In most aptasensors described for the determination of small molecules, CNTs are used as supports for the immobilization of aptamers and auxiliary reagents required for signal detection. It should be noted that CNTs themselves have electric conductivity typical rather for semiconductors than for metals. Thus, their deposition on the electrode does not obligatory follow improved parameters of the electron transfer. Increased currents recorded by voltammetric techniques (DC voltammetry, DPV, SWV, etc.) are mostly related to the increased surface of the working electrode. This effect is quantified by the peak currents of the redox probe (commonly $[Fe(CN)_6]^{3-/4-}$) in accordance with the Randles–Sevcik equation. In many aptasensors described, the authors used additional materials with a higher conductivity, such as Au or Pt nanoparticles or polyaniline, that compensate for the modest conductivity of the CNTs and provide better shape of the peaks and lower contribution of the resistance to the electron transfer at the electrode interface. However, even non-conductive materials such as ferrites or metal oxides, which cannot participate in the chain of the electron transfer often improve the characteristics of electrochemical aptasensors with CNTs due to improved mechanical properties of the surface layer and stabilization of the porous 3D structure of the CNTs net promising both high permeability for the charge transfer carriers and electric wiring of the aptamers with electrode. The authors announce a synergetic effect of such materials but few of them provided the results obtained with applied auxiliary non-conductive compounds with no CNTs. To some extent, the tradition of application of metal oxides appeared from other examples of aptasensing that employed fluorescence signal (carbon and metal nanodots, graphene nanoflakes) or magnetic separation of biochemical reactants in conventional immunoassay (ferromagnetic species). Explaining the need in such auxiliary components of the CNTs layer, the authors refer to their strong mechanical, magnetic, semiconductor and other properties [135,149–151] that make sense in other protocols of signal measurement and are then transferred to the area of "pure" electrochemical analysis. In many cases, such a strategy works, but the results should depend on the size distribution of both CNTs and no-conductive electrochemical inactive components.

Table 1. Characteristics of electrochemical aptasensors based on CNTs (2016–2020).

Target	Surface Layer Content	Signal Measurement Protocol	Linearity Range/LOD	Ref.
Aflatoxin B1	Au electrode covered with nafion-chitosan film. Capturing DNA probe is covalently attached to the surface via glutaraldehyde binding. Aptamer modified with CNTs is immobilized by hybridization	EIS measurements of charge transfer resistance	0.15–10 nM, LOD 0.074 nM	[117]
Bisphenol A	GCE covered with carboxylated MWCNTs-chitosan composite. Aminated DNA strand is covalently attached via carbodiimide binding and ferrocene labeled aptamer by hybridization	DPV current of the ferrocene redox label	0.2–2.0 nM, LOD 0.38 nM	[152]
	Au screen-printed electrode covered with carbon tape and physically adsorbed MWCNTs covered with Au layer. Pinhole aptamer covalently attached to Au via terminal -SH group	Aptamer is saturated with the MB molecules, analyte released MB from the surface layer so that its signal recorded with SWV decreases with bisphenol A concentration	10 fM–1 nM, LOD 8 fM	[135]
	GCE covered with MWCNTs covered with thiolated magnetic particles of $CuFe_2O_4$ bearing Au nanoparticles and aptamer	DPV current of the $[Fe(CN)_6]^{3-/4-}$ redox indicator	0.05–9 nM, LOD 25 pM	[153]
	GCE covered with carboxylated MWCNTs modified with poly(ethylene imine), Pt nanoparticles and capturing DNA probe complementary to the aptamer	DPV current of the $[Fe(CN)_6]^{3-/4-}$ redox probe	1–400 nM, LOD 210 pM	[149]
	GCE covered with carboxylated MWCNTs modified with Prussian blue and Au nanoparticles and covalently attached capturing DNA hybridized with the aptamer	EIS measurements of charge transfer resistance	0.1–1 pM and 10 pM–10 nM, LOD 0.045 pM	[154]
Ceruloplasmin	GCE covered with MWCNTs, treated with diazonium salt and aminated aptamer was immobilized by carbodiimide binding	DPV current of the $[Fe(CN)_6]^{3-/4-}$ redox indicator	0.02–3.0, 3.0–80 ng/mL, LOD 3.7 pM	[155]
Chlorpyrifos	GCE covered with nafion and carboxylated SWCNTs with the CuO nanoflowers. Aminated capturing probe is attached to carboxylic groups by carbodiimide binding, signaling aptamer is hybridized with capturing probe and then saturated with MB	DPV measurements of the MB released in target interaction so that its signal decreases with the chlorpyrifos concentration	0.1–150 ng/mL, LOD 70 pg/mL	[156]
Ciprofloxacin	Screen-printed carbon electrode modified with MWCNTs–V_2O_5–chitosan composite. Aminated aptamer immobilized by carbodiimide binding	EIS measurements of relative shift of the charge transfer resistance	0.5–8.0 ng/mL, LOD 0.5 ng/mL	[157]
Codeine	GCE covered with MWCNTs modified with aminated Fe_3O_4-Au composite, aminated aptamer is linked to the composite by glutaraldehyde	DPV current of the $[Fe(CN)_6]^{3-/4-}$ redox indicator	0.01–1 and 10–900 nM, LOD 3.2 pM	[150]
Diclofenac	GCE covered with carboxylated MWCNTs followed by electrodeposition of Ag-Pt nanoparticles. Aminated capturing DNA is immobilized by carbodiimide binding, complementary DNA by hybridization	EIS measurements of charge transfer resistance	10 pM–800 nM, LOD 2.8 pM	[158]
Dopamine	GCE covered with carboxylated MWCNTs and electrodeposited Pt and Au nanoparticles. Aminated capturing DNA strand immobilized by carbodiimide binding, complementary aptamer by hybridization	Aptamer is saturated with the MB molecules, analyte released MB from the surface layer so that its signal recorded with DPV decreases with dopamine concentration	1–30 nM, LOD 0.22 nM	[159]
	Au electrode modified with Au nanoparticles and carboxylated MWCNTs, aminated capturing DNA strand is immobilized by carbodiimide binding and complementary aptamer by hybridization	Aptamer is saturated with the MB molecules, analyte released MB from the surface layer so that its signal recorded with DPV decreases with dopamine concentration	5–300 nM, LOD 2.10 nM	[160]
	GCE covered with carboxylated MWCNTs and chemically synthesized Au nanoparticles and Prussian blue in chitosan matrix. Aptamer immobilized by carbodiimide binding	DPV measurement of the Prussian blue signal decreasing with dopamine concentration	0.50–50.0 nM, LOD 0.2 nM	[161]
Epirubicine	Carboxylated MWCNTs attached to GCE are treated with ethylene diamine and then covered with Au nanoparticles. Thiolated aptamer immobilized by Au-SH binding	DPV measurement of the curcumin signal after addition of the DNA strand complementary to the aptamer	0.007–7.0 μM, LOD 3.0 nM	[162]

Table 1. *Cont.*

Target	Surface Layer Content	Signal Measurement Protocol	Linearity Range/LOD	Ref.
17β-Estradiol	Origami paper folded planar electrode with microfluidic channels modified with aminated SWCNTs, Au nanoparticles and New Methylene Blue redox indicator. Aptamer immobilized via terminal SH group	DPV signal of New Methylene Blue redox indicator	10–500 pg/mL, LOD 5 mg/mL	[163]
	GCE covered with MWCNTs with adsorbed thionine and Au nanoparticles, thiolated aptamer immobilized via Au-SH binding	DPV measurement of thionine and estradiol oxidation peaks	12 pM–60 nM, LOD 1.5 pM	[164]
Furaneol	Silver electrode covered with monolayer of cysteamine followed by CNTs immobilization and covalent attachment of capturing DNA strand hybridized with the aptamer nearing Methylene blue as redox indicator	Displacement protocol with SWV determination of decreasing signal of Methylene blue oxidation	1 fM–35 μM, LOD 0.557 fM	[165]
Ibuprofen	GCE covered with MWCNTs treated with terephtalaldehyde. Aminated capturing DNA strand is immobilized by carbodiimide binding and complementary aptamer by hybridization.	Aptamer is saturated with the MB molecules, analyte released MB from the surface layer so that its signal recorded with DPV decreases with ibuprofen concentration	70 pM–6 μM, LOD 20 pM	[166]
Kanamycin	GCE covered with MWCNTs suspension of $MoSe_2$ nanoflowers and MWCNTs followed by electrodeposition of Au nanoparticles. Aptamer immobilized by carbodiimide binding	EIS measurements of charge transfer resistance	1 pM–0.1 nM, 100 nM–10 μM, LOD 0.28 pM	[167]
Malathion	Fluorine tin oxide sheet covered with PEDOT and carboxylated MWCNTs composite, aminated aptamer covalently attached onto the layer	DPV measurement of intrinsic PEDOT activity	0.1 fM–1 μM, LOD 0.1 fM	[168]
Mucin	Screen-printed carbon electrode covered with MWCNTs treated with diazonium salt. Aminated aptamer immobilized to the benzoic acid residues by carbodiimide binding	EIS measurements of relative shift of the charge transfer resistance	0.1–2 U/mL, LOD 0.02 U/mL	[169]
Myoglobin	GCE covered with MWCNTs and chemically synthesized Pt-Sn nanoparticles. Aminated aptamer immobilized by carbodiimide binding	DPV current of the $[Fe(CN)_6]^{3-/4-}$ redox indicator	0.01–1 nM, 10–200 nM, LOD 2.2 pM	[170]
Nitenpyram	GCE covered with bilayer of hydroxylated MWCNTs ad carbon nanohorn particles	DPV measurement of the analyte reduction peak current	20–2000 nM, LOD 40 nM	[171]
Oxytetracycline	Thin-film planar Au electrode with thiolated DNA strand. Carboxylated MWCNTs with adsorbed thionine and Au nanoparticles bearing aptamer are attached to the surface via hybridization of the aptamer with capturing DNA strand	DPV current of thionine oxidation	1×10^{-13}–1×10^{-5} g/mL, LOD 3.1×10^{-14} g/mL	[172]
Potassium ion	Field effect transistor with SWCNT as a gate and aptamer immobilized via 1-pyrene butanoic acid	Changes in conductivity of SWCNT	1 pM–11 nM, LOD 10 pM	[173]
Profenofos	Screen-printed electrode modified with graphitized MWCNTs and Au nanoparticles. Thiolated or aminated aptamers are immobilized by covalent bonds formed in carbodiimide binding or Au-SH interactions	DPV current of the $[Fe(CN)_6]^{3-/4-}$ redox indicator	0.1–1×10^5 ng/mL, LOD 0.052 ng/mL	[174]
Prostate specific antigen (PSA)	GCE covered with carboxylated MWCNTs in chitosan matrix. Aminated capturing DNA strand is immobilized by glutaraldehyde binding and complementary aptamer by hybridization	Aptamer is saturated with the MB molecules, analyte released MB from the surface layer so that its signal recorded with DPV decreases with PSA concentration	0.85–12.5, 12.5–500 ng/mL, LOD 0.75 ng/mL	[118]
Salmonella	Indium-Tin Oxide (ITO) electrode covered with carboxylated MWCNTs followed by covalent attachment of aminated aptamer by carbodiimide binding	EIS measurements of charge transfer resistance	LOD 55 CFU/mL and 67 CFU/mL for *S. Enteritidis* and *S. Typhimurium*,	[175]
Saxitoxin	Carboxylated MWCNTs are physically adsorbed on the Au electrode modified with octadecanethiol. MB is electrostatically adsorbed onto the MWCNTs layer and aminated aptamer immobilized by carbodiimide binding.	DPV measurement of the MB signal decrease	0.9–30 nM, LOD 0.38 nM	[176]

Table 1. *Cont.*

Target	Surface Layer Content	Signal Measurement Protocol	Linearity Range/LOD	Ref.
Streptomycin	GCE covered with MWCNTs-chitosan composite with implemented Pd nanoparticles. Aminated aptamer is immobilized by glutaraldehyde binding	EIS measurements of charge transfer resistance	0.1–1500 nM, LOD 18 pM	[177]
	GCE covered with MWCNTs decorated with Fe_3O_4-Au nanoparticles and nanoporous Pt-Ti alloy	DPV current of the $[Fe(CN)_6]^{3-/4-}$ redox indicator	0.05–100 ng/mL, LOD 7.8 pg/mL	[178]
	GCE covered with porous carbon nanorods and MWCNTs bearing CuO and Au nanoparticles. Thiolated aptamer is immobilized via Au-SH binding	DPV current of the $[Fe(CN)_6]^{3-/4-}$ redox indicator	0.05–300 ng/mL, LOD 0.036 ng/mL	[179]
Sulfadimidine	Bare Au electrode modified with 2-aminoethanethiol and MWCNTs decorated with Au nanoparticles. Thiolated aptamer was immobilized via Au-SH binding	DPV current of the $[Fe(CN)_6]^{3-/4-}$ redox indicator	0.1–50 ng/mL, LOD 0.055 ng/mL	[180]
Tetracycline	GCE covered with MWCNTs with adsorbed thionine and Au nanoparticles. Thiolated capturing DNA strand is immobilized via Au-SH binding and aptamer by hybridization	DPV measurement of thionine oxidation	0.1 nM–1 µM, LOD 0.06 nM	[181]
	GCE covered with MWCNTs and electropolymerized L-glutamic acid, aminated aptamer immobilized by carbodiimide binding	EIS measurements of charge transfer resistance	1.0×10^{-16}–1.0×10^{-6} M), LOD 3.7×10^{-17} M	[182]
	Interdigitated microelectrode array covered with MWCNTs in chitosan matrix, aptamer is physically adsorbed on the surface layer	EIS measurements of charge transfer resistance	1.0 nM–1.0 mM	[183]
Thrombin	GCE covered with suspension of the MWCNT-TiO_2 composite, chitosan and 3-[(2-hydroxypropyl)imino]in- doline-2-one. Aptamer is physically adsorbed on the surface layer	DPV current of the $[Fe(CN)_6]^{3-/4-}$ redox indicator	0.00005–10 nM, LOD 1.0 fM	[184]
	GCE covered with MWCNTs, which were previously modified with chemically either electrochemically synthesized polyaniline. Thiolated aptamer is physically adsorbed on the surface layer	Changes in intrinsic redox activity of polyaniline measured by peak currents on cyclic voltammogram	0.0001–4 nM, LOD 0.08 pM	[185]
Tryptophan	Graphite screen-printed electrode modified with MWCNTs-chitosan composite and Au nanoparticles. Thiolated capturing DNA strand is immobilized via Au-SH binding and aptamer by hybridization	Changes in the DPV peak of redox indicator ($[Fe(bpy)_3](p\text{-}CH_3C_6H_4SO_2)_2$)	3.0 nM–100 µM, LOD 1.0 nM	[186]
	Au electrode modified with MWCNTs; aptamer physically adsorbed on the surface layer	Potentiometric stripping analysis of tryptophan signals	1.0×10^{-10}–1.0×10^{-5}, 1.0×10^{-5}–3.0×10^{-4} M, LOD 6.4 10^{-11} M	[187]
	Golden screen-printed electrode modified with MWCNTs	Potentiometric stripping analysis of tryptophan signals	1.0×10^{-11} -1.0×10^{-4} M, LOD 4.9×10^{-12} M	[188]
Urea	GCE covered with MWCNTs with electrochemically deposited Au nanoparticles. Thiolated aptamer with urea immobilized on the Au by Au-SH binding. Then, dopamine was electropolymerized and urea removed	EIS measurements of charge transfer resistance	0.005–0.1 nM, 1.00–500 nM, LOD 900 fM	[189]
Zearalenon	Au electrode covered with PEI-MoS_2-MWCNTs composite and Pt@Au nanoparticles followed by thiolated aptamer immobilization	Toluidine blue (redox indicator) signal measured by cyclic voltammetry	0.5 pg/mL–50 ng/mL, LOD 0.17 pg/mL	[190]

This might result in a higher deviation of the signal and the necessity to use relative parameters such as the sight of the signal against blank experiment or against its maximal deviation within the analyte concentration range considered. The same can be referred to the use of surfactants and polyelectrolytes, which simplify the dispersion of CNTS and improve the stability of appropriate suspensions, especially those used as redox indicator carriers.

Au nanoparticles obtained electrochemically or chemically on the CNTs support play anchoring role for immobilization of the aptamers with terminal SH-group. They increase the density of the aptamers on the electrode surface against bare gold and in some cases result in more regular coating required in the label-free impedimetric detection of the signal. It should be noted that the use of CNTs as templates in the synthesis of metal nanoparticles improves their morphology and makes even the size distribution against the same process on bare electrode. This is another argument in favor of the use of CNTs prior to metal deposition.

4.2. Graphene Materials

As was mentioned above, rGO is mainly used for the aptasensor assembling. Its following reduction by cathodic polarization or chemical treatment retains a certain number of functional groups for aptamer immobilization. It should also be noted that graphene itself is rather hydrophobic and easily loses its excellent properties due to reverse amalgamation to graphite-like nanostructures. For this reason, the selection of solvents for suspending graphene materials and electrolyte content can significantly alter the aptasensor performance. Doping graphene with heteroatoms improves its properties in the aptasensor assembly. Together with partial oxidation and amination, this makes it possible to change main characteristics of the surface charge and durability of the coating. Graphene materials are easily combined with other carbon nanomaterials that are retained in the composites by π–π stacking interactions of aromatic systems. In such complexes, the individual characteristics of additives, as a rule, retained and can be used for the following immobilization of aptamer via Au–SH interactions or carbodiimide binding. Aminated and carboxylated graphene particles are also implemented in polyelectrolyte complexes. Interestingly, the adsorption of organic dyes onto graphene sheets is quite effective and a reliable way to implement them as redox labels together with aptamers or auxiliary DNA strands. Separation of the reactants (dyes on graphene and aptamer on Au nanoparticles) does not alter the sensitivity of the measurement by making aptasensor assembling easier. Graphene materials can also serve as templates for electropolymerization. In addition to the electric wiring and providing immobilization support, the products of electropolymerization make the interface more hydrophilic and improve the reproducibility of EIS measurements based on the transfer of small multiply charged $[Fe(CN)_6]^{3-/4-}$ on the graphene interface. Contrary to CNT-based aptasensors, the signal of aptasensors based on graphene materials is less sensitive to non-specific adsorption of the real sample components. The necessity to block bare surface of the electrode or to treat them with bovine serum albumin (BSA) or surfactants is not obligatory and can be often omitted. The application of graphene materials in the assembly of electrochemical aptasensors is summarized in Table 2 for the period from 2016 to 2020.

4.3. Other Carbon Nanomaterials

The examples of the application of g-carbon nitride, carbon black, fullerene and related materials in electrochemical aptasensors are presented in Table 3.

g-C_3N_4 particles are mostly obtained from melamine though there are many other nitrogen containing organic compounds applicable as their sources. The structure, electroconductivity and purity of the product highly depend on the conditions of pyrolysis and calcination and vary from one article to another one. This variability offers additional possibilities to affect the aptasensor performance but is still rarely used compared with CNTs or graphene materials. Carbon nitride has never been used alone in the aptasensor assembly. It is involved in various composite materials that mostly include metal oxides, graphene nanosheets, Au and Ag nanoparticles.

Table 2. Characteristics of electrochemical aptasensors based on graphene and related materials (2016–2020).

Target	Surface Layer Content	Signal Measurement Protocol	Linearity Range/LOD	Ref.
Acetamiprid	Graphene quantum dots (QDs) modified with histidine are bound on graphite oxide on GCE and treated with Ag^+ ions to form silver nanoparticles followed by covalent immobilization of thiolated aptamer via Ag-SH binding	DPV signal of ferricyanide redox indicator	1.0×10^{-16}–5.0×10^{-12} M, LOD 4.0×10^{-17} M	[191]
Aflatoxin B1	GCE covered with alternated layer of *N*-doped graphene, carboxylated polystyrene and PDDA, aptamer attached by carbodiimide binding	EIS measurements of the relative shift of the charge transfer resistance	0.001–0.1 ng/mL, LOD 0.002 ng/mL	[192]
Carcinoembryonic antigen (CEA)	GCE electrografted with *p*-nitrophenyldiazonium cation reduced to aminophenyl monolayer, GO deposited onto the layer and then cathodically reduced	Homogeneous aptamer-based assay based on T7 exonuclease (T7Exo)-assisted target analog recycling and detection of the Methylene blue labels in the synthesized long single stranded DNA	80 ag/mL–950 fg/mL, LOD 80 ag/mL	[193]
	GCE covered with *N*-doped graphene decorated with Au nanoparticles; graphene QDs are deposited on the surface and capturing DNA strand is immobilized via carbodiimide binding. Signaling aptamer is attached to hemin aptamer by glutaraldehyde	Aptasensor is consecutive treated with analyte and hemin-signaling aptamer conjugate. After sandwich complex formation, peroxidase like activity of hemin is measured by DPV in the presence of hydrogen peroxide	1.0×10^{-5}–200.0 ng/mL, LOD 3.2 fg/mL	[194]
Digoxin	Au screen-printed electrode modified with Au nanoparticles with monolayer of mercaptopropionic acid, aminated aptamer immobilized via carbodiimide binding. Composite of Ag nanoparticles GO was adsorbed onto the aptamer as redox indicator	DPV measurement of Ag nanoparticles dissolution	1 pM–1 μM, LOD 0.3 pM	[136]
Dopamine	GCE covered with collagen–GO composite, aptamer physically adsorbed on the composite layer	DPV signal of dopamine	1–1000 nM, LOD 0.75 nM	[195]
	GCE covered with GO followed by Nile blue adsorption and Au nanoparticles deposition. Thiolated aptamer immobilized by Au-SH binding	DPV signal of dopamine and Nile blue as redox indicator	10 nM–0.2 mM, LOD 1 nM	[196]
Liposaccharides	GCE modified with rGO and Au nanoparticles. Aptamer immobilized by Au-SH binding	SWV and EIS measurements with ferrocyanide redox indicator, SWV of Mg containing carbon dots	0.1–0.9 pg/mL, LOD 1 fg/mL	[121]
Lysozyme	GCE covered with rGO-chitosan-carbon dots composite and covalently attached aminated aptamer	DPV and EIS measurement of the ferricyanide redox indicator signal	20 fM–10 nM (DPV), 10 fM–100 nM (EIS), LOD 3.7 fM (DPV), 1.9 fM (EIS)	[122]
Mucin	Fluorine tin oxide electrode modified with Au nanoparticle, GO and electropolymerized PEDOT layer; aptamer immobilized by avidin-biotin interaction	DPV current of the $[Fe(CN)_6]^{3-/4-}$ redox indicator	3.13 aM–31.25 nM, LOD 0.031 fM	[197]
Myoglobin	Indium-tin oxide (ITO) electrode modified with rGO modified with poly(ethylene imine) and electrostatically accumulated aptamer	DPV reduction peak referred to the myoglobin redox activity	0.001–1000 ng/mL, LOD 0.97 pg/mL	[198]
Ochratoxin A	Indium-tin oxide (ITO) electrode covered with rGO covalently attached to chitosan by carbodiimide binding, aptamer immobilized by streptavidin-biotin interaction	DPV current of the $[Fe(CN)_6]^{3-/4-}$ redox indicator	0.01 ng/mL–100 fg/mL, LOD 1 fg/mL	[199]
Organophosphate pesticides	Screen-printed carbon electrode with electrodeposited layer of GO and aminated aptamer and Cu nanoparticles	DPV current of the $[Fe(CN)_6]^{3-/4-}$ redox indicator	0.01–100 (profenofos), 1–1000 (phorate), 0.1–1000 (isocarbophos) and 1–500 nM (omethoate), LOD 0.003 (profenofos), 0.3 (phorate), 0.03 (isocarbophos) and 0.3 nM (omethoate)	[123]

Table 2. *Cont.*

Target	Surface Layer Content	Signal Measurement Protocol	Linearity Range/LOD	Ref.
Pb^{2+}	GCE covered with capturing Au–MoS_2–rGO nanocomposite and thiolated capturing aptamer hybridized with DNAzyme bearing metal-organic framework with AuPd nanoalloy particles	DPV signal of electrocatalytic reduction of H_2O_2 decreasing with increased Pb^{2+} concentration due to cleavage of the aptamer strand and removal of metal nanoparticles	5.0 pM–2.0 μM, LOD 0.07 pM	[200]
Thrombin	GCE covered with rGO and Au nanoparticles, Then, thiolated aptamer was mixed with thrombin and immobilized by Au-SH binding. Finally, thionine was electropolymerized and template washed out	DPV signal of polythionine	2.5×10^{-9}–1.3×10^{-6} mg/mL, LOD 1.6×10^{-10} mg/mL	[124,125]
	Au microelectrode modified with thiolated capturing aptamer, signaling aptamer attached to the rGO - Ag nanoparticle composite	DPV signal of Ag nanoparticles recorded after formation of sandwich complex capturing aptamer - thrombin - signaling aptamer	0.05–5 nM, LOD 0.03 nM	[201]
	GCE covered GO with covalently attached double-stranded DNA decorated with electrodeposited Au nanoparticles and immobilized thiolated aptamer	EIS measurements of charge transfer resistance	0.1–100 nM, LOD 0.06 nM	[202]
Tuberculosis antigen ESAT-6	GCE with deposited rGO doped with metal-organic framework and adsorbed toluidine blue. Thiolated aptamer immobilized onto the Pt@Au nanoparticles	DC voltammetry measurements of toluidine blue redox peak currents	1.0×10^{-4}–2.0×10^{2} ng/mL, LOD 3.3×10^{-5} ng/mL	[203]
Zearalenon	Au electrode covered with Pt nanotubes, nafion and thiolated aptamer. Thionine labeled GO physically adsorbed on the aptamer layer	DPV measurement of the thionine oxidation current	0.0005–500 ng/mL, LOD 0.000167 ng/mL	[137]
	Aptasensors on graphene–CNTs composite			
Cancer antigen CA125	rGO deposited in the gate of the field effect transistor and covered with carboxylated MWCNTs nearing aptamer	Shift of the drain-source current	1.0×10^{-9}–1.0 U/mL, LOD 5.0×10^{-10} U/mL	[146]
Carcinoembryonic antigen (CEA)	GCE covered with rGO, hemin and MWCNTs, thiolated aptamer immobilized by Au-SU binding	DPV measurement of hemin redox activity	1.0 fg/mL–10 ng/mL, LOD 0.68 fg/mL	[204]
Diazinon	GCE covered with VS_2 quantum dots-graphene nanoplateles and carboxylated MWCNTs	DPV signal of ferricyanide redox indicator and EIS measurement of charge transfer resistance	5.0×10^{-14}–1.0×10^{-8} (DPV), 1.0×10^{-14}–1.0×10^{-8} M (EIS), LOD 1.1×10^{-14} (DPV) and 2.0×10^{-15} M (EIS)	[205]
Diclofenac	GCE covered with the mixture of GO, Fe_3O_4 and MWCNTs, preliminary heated and autoclaved. Aminated aptamer immobilized by carbodiimide binding	DPV current of the $[Fe(CN)_6]^{3-/4-}$ redox indicator	100–1300 p[M, LOD 33 pM	[206]
Dopamine	GCE covered with composite obtained by mixing GO, MWCNTs and Ag nanoparticles, aptamer immobilized by carbodiimide binding	DPV current of the $[Fe(CN)_6]^{3-/4-}$ redox indicator	3–110 nM, LOD 0.7 nM	[207]
Edifenphos	GCE covered with GO-carboxylated MWCNTs and then polarized to reduce GO into rGO, aminated aptamer immobilized by carbodiimide binding	DPV current of the $[Fe(CN)_6]^{3-/4-}$ redox indicator	0.001–1300 nM, LOD 0.1 pM	[208]
Lysozyme	GCE covered with GO and MWCNTs films decorated with Au nanoparticles taken in various combinations	EIS measurements of the charge transfer resistance shift	0.02–250 pM, LOD 9 fM (for the best content of the layer)	[209]
Oxaliplatin	GCE covered with rGO and carboxylated MWCNTs followed by deposition of Au-Pd nanoparticles and aminated aptamer immobilized by carbodiimide binding	EIS measurements of the charge transfer resistance shift	0.1–170 nM, LOD 60 pM	[210]
Platelet-derived growth factor-BB	CGE covered with Se doped graphene–MWCNTs suspension followed by electrodeposition of Au nanoparticles and attachment of capturing hairpin aptamer	Interaction of the aptamer resulted in opening hairpin structure and interaction with two auxiliary sequences to form Y-junction DNA that released analyte and bonded hemin molecules generating DPV signal	0.0001–10 nM, LOD 27 fM	[145]

Table 2. *Cont.*

Target	Surface Layer Content	Signal Measurement Protocol	Linearity Range/LOD	Ref.
Prostate specific antigen (PSA)	GCE covered with GO-carboxylated MWCNTs composite then polarized to reduce GO into rGO and decorated with Au nanoparticles, thiolated aptamer immobilized by Au-SH binding	DPV and EIS measurement of the $[Fe(CN)_6]^{3-/4-}$ redox indicator signal	0.005– 20 ng/mL (DPV) and 0.005–100 (EIS) ng/mL, LOD 1.0 pg/mL	[211]
Salmonella ATCC 50761	GCE covered with GO-carboxylated MWCNTs composite then polarized to reduce GO into rGO, aminated aptamer immobilized by carbodiimide binding	EIS measurements of the charge transfer resistance shift	75–7.5 × 10^5 CFU/mL, LOD 25 CFU/mL	[212]
Salmonella enterica	GCE covered with rGO-MWCNTs composite prepared by hydrothermal method, aminated aptamer immobilized by carbodiimide binding	DPV current of the $[Fe(CN)_6]^{3-}$ redox indicator	10–10^8 CFU/mL, LOD 10 CFU/mL	[213]
Sulfamethazine	Bare Au electrode covered with suspension of GO and carboxylated MWCNTs followed by electrodeposition of Au nanoparticles and immobilization of thiolated aptamer by Au-SH binding	DPV current of the $[Fe(CN)_6]^{3-/4-}$ redox indicator	0.01–50 ng/mL, LOD0.0052 ng/mL	[138]

Table 3. Characteristics of electrochemical aptasensors based on other carbon nanomaterials (2016–2020).

Target	Surface Layer Content	Signal Measurement Protocol	Linearity Range/LOD	Ref.
	$g\text{-}C_3N_4$			
Amoxicillin	GCE covered with TiO_2-$g\text{-}C_3N_4$ composite obtained by hydrothermal method from $(NH_4)_2TiF_6$, glucose and melamine. Then, Au nanoparticles were electrochemically deposited and thiolated aptamer immobilized by Au-SH binding	EIS measurements of the charge transfer resistance shift	0.5–3 nM LOD 0.2 nM	[214]
Cadmium (II)	GCE covered with the mixture of rGO and $g\text{-}C_3N_4$, aminated aptamer immobilized by carbodiimide binding	Differential anodic stripping voltammetry signal	1 µM–1 mM, LOD 0.337 nM	[215]
Ochratoxin A	Au electrode covered with a monolayer of capturing single-stranded DNA complementary to aptamer immobilized by hybridization. In target reaction, aptamer interacts with the analyte and leaves the electrode surface	$g\text{-}C_3N_4$ interacted with single DNA strand and catalyzed H_2O_2 oxidation monitored by DC voltammetry	0.2–500 nM, LOD 0.073 nM	[139]
Prostate specific antigen	Au electrode modified with nanocomposite of MoS_2 quantum dots and $g\text{-}C_3N_4$ nanosheets obtained by hydrothermal method from melamine and decorated with chitosan-stabilized Au nanoparticles. Thiolated aptamer immobilized by Au-SH binding	EIS measurements of the charge transfer resistance shift	1 pg/mL–1.0 ng/mL, LOD 0.71 pg/mL	[216]
Thrombin	GCE covered with $g\text{-}C_3N_4$ from melamine decorated with chemically synthesized Ag nanoparticles. Thiolated aptamer immobilized by Ag-SH binding	EIS measurements of the charge transfer resistance shift	100 fM–20 nM, LOD 38 fM	[217]
	Fullerene			
Prostate specific antigen (PSA)	Screen-printed carbon electrode covered with MWCNTs and C_{60}-chitosan–ionic liquid composite. Au nanoparticles electrochemically deposited onto the layer, thiolated aptamer immobilized by Au-SH binding	DPV and EIS measurement of the $[Fe(CN)_6]^{3-/4-}$ redox indicator signal	1–200 (EIS), 2.5–90 (DPV) pg/mL, LOD 0.5 (EIS), 1.5 (DPV) pg/mL	[218]
Sulfadimethoxine	Au electrode modified with thiolated capturing DNA strand and complementary aptamer, rGO-C_{60} nanohybrid with physically adsorbed toluidine blue used as a terminal label of signaling FNA strand	Analyte mixed with RecJf exonuclease initiates catalytic cycle resulted in removal aptamer from the electrode interface, after that, toluidine blue signal was measured using DPV technique	10 fg/mL–10 ng/mL, LOD 10 fg/mL	[140]

Table 3. *Cont.*

Target	Surface Layer Content	Signal Measurement Protocol	Linearity Range/LOD	Ref.
	GCE covered with PDDA modified C_{60} and rGO, physically adsorbed glucose oxidase and Pt@Au–C_{60}–rGO nanocomposite with thiolated capturing aptamer immobilized by Au-SH binding	DPV measurement of direct electron transfer to glucose oxidase	10 fg/mL–50 ng/mL, LOD 8.68 fg/mL	[219]
2,4,6-Trinitrotoluene	GCE consecutively covered with C_{60}, Au nanoparticles and thiolated aptamer	EIS measurements of the charge transfer resistance shift	0.50 fM–5 μM, LOD 0.17 fM	[220]
Tuberculosis antigen MPT-64	GCE covered with Fe-containing metal-organic framework particles modified with poly(ethylene imine) and Au nanoparticles, thiolated aptamer immobilized via Au-SH binding	Sandwich assay with signaling aptamer modified with C_{60}-GO-*N*-doped CNTs composite. DPV signal of C_{60}	1–10^6 fg/mL LOD 0.33 fg/mL	[221]
	GCE covered with thiolated capturing aptamer	Sandwich assay with polyaniline–C_{60} composite decorated with Au nanoparticles bonded to signaling aptamer. DPV signal of ascorbic acid reducing polyaniline	0.02–1000 pg/mL, LOD 20 fg/mL	[222]
Carbon black, CDs and related nanomaterials				
Bisphenol A	GCE covered with *N*,*S*,*P*-doped CDs obtained by hydrothermal method from cucumber juice, chemically synthesized Au nanoparticles and thiolated aptamer	DPV and EIS measurement of the $[Fe(CN)_6]^{3-/4-}$ redox indicator signal	0.01 -120 μM, LOD 0.53 nM	[223]
Cadmium(II)	Screen-printed carbon electrode with drop casted carbon black, electrodeposited Au nanoparticles and thiolated aptamer immobilized by Au-SH binding	SWV measurement of the $[Fe(CN)_6]^{3-/4-}$ redox indicator signal	1 50 ppb, LOD 0.14 ppb	[224]
Chlorpyrifos	GCE covered with CB in chitosan matrix, GO@Fe_3O_4 prepared by solvothermal method and physically adsorbed aptamer	DC voltammetry measurement of the $[Fe(CN)_6]^{3-/4-}$ redox indicator signal	0.1–10^5 ng/mL, LOD 0.033 ng/mL	[225]
Insulin	GCE covered with CDs obtained from candle soot and dispersed in chitosan. Aminated aptamer immobilized by glutaraldehyde cross-linking	EIS measurements of the charge transfer resistance shift	0.5–10 nM, LOD 106.8 pM	[226]
Protein tyrosine kinase-7	GCE covered with porous amorphous carbon - MnO_2/Fe_2O_3 composite followed by aptamer covalent attachment	EIS measurements of the charge transfer resistance shift	0.0001–10 ng/mL, LOD 44 fg/mL	[227]
Tobramycin	Au electrode covered with suspension of carbon nanospheres embedded with SnO_x@TiO_2 obtained by calcination of the mixture of bovine serum albumin, Na_2SnO_3 and butyl titanate. Aptamer immobilized by electrostatic adsorption	EIS measurements of the charge transfer resistance shift	0.01–5 ng/mL, LOD 6.7 pg/mL	[228]

Metal oxides can be obtained "in one pot" with g-C_3N_4 particles by mixing appropriate precursors and their heating in autoclave. As a sign of the 'green chemistry' approach, biomasses and agriculture wastes can be used [229].

Other carbon nanomaterials mentioned here are also applied mostly as auxiliary components of the surface layer required for the control of the density, mesoporous structure and roughness of the coating. They are always combined with other modifiers and are not used alone. Due to their own size being much lower than that of CNTs or graphene nanosheets, carbon nitride, carbon dots and carbon black do not predetermine the properties of the surface layer but improve some of the existing ones, such as permeability for small ions or increased adsorption capacity. To some extent, carbon black and carbon dots can be considered as a less expensive alternative to graphene and CNTs, although, at present, economic factors do not play a significant role in the biosensors production. The cost of carbon materials always remains much lower than that of biochemicals required (aptamers, capturing DNA strands etc.). Except CDs and fullerene, they are rarely applied in microsensors because of diversity of properties and irregular content of many industrial samples. On the other hand, easy synthesis of complex multicomponent composites by the hydrothermal method offers opportunities for extending the number of such compounds available for aptasensor development.

It is important to note that the sensitivity of most of the aptasensors based on carbon nanomaterials is extremely high and meets most requirements of medical diagnostics and environmental monitoring. Moreover, in some cases concerning the determination of organophosphate pesticide, the concentrations determined are so small that it is hard to find the analytical problems corresponding to their value. Indeed, the detection of profenofos on the level of 0.025 ng/mL [174] or malathion on the level of 0.1 fM [168] does not have sense in terms of food safety or contamination assessment. To some extent, this also refers to the determination of some metabolites, such as trypthophan and urea. One of the possible reasons to reach lower and lower LOD values is to allow for a higher dilution of the samples and hence suppress matrix interference. However, in other cases, especially for cancer biomarker detection, the extremely high sensitivity of the aptasensrs described seems an important advantage due to opportunities of early diagnosis of cancer diseases and hopes for more successful therapy of such patients. Regarding relative influence of different modifiers on the analytical performance of aptasensors, only a few analytes have been determined with various content of the surface layer. Some of such works (see determination of thrombin and CEA) were performed in the same research groups with rather insignificant changes of the measurement conditions. It can be concluded from the comparison of these results that the use of carbon nanomaterials in combination with Au nanoparticles or other catalytic systems provides better performance against 'pure' carbon nanomaterial. Then, the biochemical amplification mechanism also increased the sensitivity of the assay, even to a higher extent than the inclusion of additional inorganic components into the aptasensor assembly. It should be noted that such systems, being very sensitive, require much more reagents and extra stages so that the duration of the measurement cycle stands to about one hour. Together with the requirements of thermosetting, this makes such measurement protocols incompatible with the biosensor idea assuming portable instrumentation with fast and rather simple measurement protocol. Such a complication of the bioassay is rational if biomarkers crucially important for danger disease diagnostics are detected. Regarding signal measurement mode, EIS shows a much higher sensitivity of the response against voltammetry though the use of DPV technique can decrease this difference to acceptable levels. Meanwhile, EIS requires careful control of non-specific adsorption and can provide positive false in the diagnostics of some biomarkers.

5. Conclusions

During the past decades, aptamers have emerged from the laboratories and have become a conventional tool of biomedical assay, especially for the detection of disease biomarkers, drug residues and environmental pollutants. Similar to the conventional immunoassay technique, aptamers are also reversibly bonded to target species, but they are more stable toward hydrolysis and oxidative damage

and can be easily modified for implementation in biosensor assembly. The number of aptamers selected for the detection of particular species is growing dramatically. However, their use in biosensors as recognition elements has some limitations related to the introduction of aptamers in the biosensors and achievement of the highest reliable signal toward a specific analyte. It should be mentioned that most of the species detected are small against the aptamer structure so that its binding results in rather modest changes of the interface conditions. To some extent, the sensitivity problem is solved by the use of aptamers changing its conformation (G_4 quadruplexes and pinhole sequences). Nevertheless, their use is especially sensitive to immobilization conditions. Taking into account the sub-nanomolar levels of analytes being detected, all above makes the development of aptasensors challenging and requires new solutions in aptasensor development and their signal optimization.

Carbon nanomaterials are considered a universal solution of many problems in biosensor design. The variety of their structure, size and morphology, unique electrical, optical and mechanical properties, and broad possibilities of functionalization and assembling in complex 3D structures make carbon nanomaterials very attractive for application in aptasensors. Numerous examples presented in the review show the diversity of approaches and achievements as a success story of aptasensors design. Many stages of the aptasensor assembling have been investigated in detail and make the process predictable and understandable. Sensitivity of detection and general usability of aptasensors become most important criteria in comparison with other analogs.

The following trends in the application of carbon nanomaterials in the electrochemical aptasensors can be emphasized:

1. Transfer from general label-free measurement protocols to more specific modes with increased reliability of the results, especially in real sample assay.
2. Synthesis and application of more complex and sophisticated materials that combine advantages of various components, e.g., electropolymerized materials, molecularly imprinted polymers, polyelectrolyte complexes on the support of carbon nanomaterials.
3. Using the simplest and most reliable approaches to the assembling of the surface layer, especially form microfluidics and microsensor devices based on carbon paper and origami constructs.
4. Varying redox labels/indicators as a route to higher robustness of the signal, especially in multicomponent samples.

In spite of diversity of publications, some problems in the design and application of aptasensors should be mentioned.

1. Few works are devoted to the multiplex assay and simultaneous determination of several analytes. Meanwhile, this might be critical for the implementation of aptasensors in diagnostic tools or environmental monitoring stations.
2. Most of the works do not consider the problems related to the changes in the aptasensor performance during the storage/operation period. Real sample assay is often presented by very simple tasks (analysis of drinking water, spiked samples of biological fluids etc.).
3. The assessment of metrological characteristics is often formal and assumes extrapolation of calibration graphs by several orders of magnitude of concentration (LOD calculation). The uncertainty in the preparation of solutions with extra-low concentration of an analyte (below 1 pM) is not considered or taken into account.
4. Most of the newly proposed aptasensors require labor- and time-consuming operation and multistep synthesis of necessary reactants. One-step measurement is the main goal and main advantage of biosensors as an alternative to conventional laboratory instrumentation.
5. The number of aptamers used in aptasensor assembly remains limited. This might result from present tasks in appropriate areas of their application, but needs further extension, meaning future progress in medicine, the food industry and environmental pollution.

Author Contributions: Conceptualization, T.H. and G.E.; methodology, A.P. and R.S.; writing—original draft preparation, T.H. and G.E.; writing—review and editing, T.H. All authors have read and agreed to the published version of the manuscript.

Funding: R.S. acknowledges support of the state subsidy in the sphere of scientific activity for Kazan Federal University (proposal No 0671-2020-0063). T.H. acknowledges funding from the Science Grant Agency VEGA, project No.: 1/0419/20.

Conflicts of Interest: The authors declare no conflict of interest.

References

1. Aceto, G.; Persico, V.; Pescapé, A. Industry 4.0 and health: Internet of things, big data, and cloud computing for healthcare 4.0. *J. Ind. Inf. Integr.* **2020**, *18*, 100129. [CrossRef]
2. Mustafa, F.; Andreescu, S. Chemical and biological sensors for food quality monitoring and smart packaging. *Foods* **2018**, *7*, 168. [CrossRef] [PubMed]
3. Ho, C.K.; Robinson, A.; Miller, D.R.; Davis, M.J. Overview of sensors and needs for environmental monitoring. *Sensors* **2005**, *5*, 4–37. [CrossRef]
4. Pendley, B.D.; Lindner, E. Medical sensors for the diagnosis and management of disease: The physician perspective. *ACS Sens.* **2017**, *2*, 1549–1552. [CrossRef] [PubMed]
5. He, J.; Li, J.; Yan, H. Environmental sensor networks: A review of critical issues. In *Advances in Multimedia, Software Engineering and Computing*; Jin, D., Lin, S., Eds.; Springer: Berlin/Heidelberg, Germany, 2011; Volume 2, pp. 425–429. [CrossRef]
6. Dincer, C.; Bruch, R.; Costa-Rama, E.; Fernández-Abedul, M.T.; Merkoçi, A.; Manz, A.; Urban, G.A.; Güder, F. Disposable sensors in diagnostics, food, and environmental monitoring. *Adv. Mater.* **2019**, *31*, 1806739. [CrossRef] [PubMed]
7. Zaukuu, J.L.Z.; Bazar, G.; Gillay, Z.; Kovacs, Z. Emerging trends of advanced sensor based instruments for meat, poultry and fish quality—A review. *Crit. Rev. Food Sci. Nutr.* **2019**, *60*, 1–18. [CrossRef] [PubMed]
8. Adley, C.C. Past, present and future of sensors in food production. *Foods* **2014**, *3*, 491–510. [CrossRef] [PubMed]
9. Primiceri, E.; Chiriacò, M.S.; Notarangelo, F.M.; Crocamo, A.; Ardissino, D.; Cereda, M.; Bramanti, A.P.; Bianchessi, M.A.; Giannelli, G.; Maruccio, G. Key enabling technologies for point-of-care diagnostics. *Sensors* **2018**, *18*, 3607. [CrossRef]
10. Walper, S.A.; Aragonés, G.L.; Sapsford, K.E.; Brown, C.W.; Rowland, C.E.; Breger, J.C.; Medintz, I.L. Detecting biothreat agents: From current diagnostics to developing sensor technologies. *ACS Sens.* **2018**, *3*, 1894–2024. [CrossRef]
11. Shrivastava, S.; Trung, T.Q.; Lee, N.-E. Recent progress, challenges, and prospects of fully integrated mobile and wearable point-of-care testing systems for self-testing. *Chem. Soc. Rev.* **2020**, *49*, 1812–1866. [CrossRef]
12. Weng, X.; Kang, Y.; Guo, Q.; Peng, B.; Jiang, H. Recent advances in thread-based microfluidics for diagnostic applications. *Biosens. Bioelectron.* **2019**, *132*, 171–185. [CrossRef] [PubMed]
13. Wu, J.; Dong, M.; Rigatto, C.; Liu, Y.; Lin, F. Lab-on-chip technology for chronic disease diagnosis. *Digit. Med.* **2018**, *1*, 7. [CrossRef] [PubMed]
14. van Reenen, A.; de Jong, A.M.; den Toonder, A.M.J.; Prins, M.W.J. Integrated lab-on-chip biosensing systems based on magnetic particle actuation—A comprehensive review. *Lab Chip* **2014**, *14*, 1966–1986. [CrossRef] [PubMed]
15. Thevenot, D.R.; Tóth, K.; Durst, R.A.; Wilson, G.S. Electrochemical biosensors: Recommended definitions and classification. *Pure Appl. Chem.* **1999**, *71*, 2333–2348. [CrossRef]
16. Clark, L.C.; Lyons, C. Electrode systems for continuous monitoring in cardiovascular surgery. *Ann. N. Y. Acad. Sci.* **1962**, *148*, 133–153. [CrossRef]
17. Chinnadayyala, S.R.; Park, K.D.; Cho, S. Review—In vivo and in vitro microneedle based enzymatic and non-enzymatic continuous glucose monitoring biosensors. *ECS J. Solid State Sci. Technol.* **2018**, *7*, Q3159–Q3171. [CrossRef]
18. Justino, C.I.L.; Duarte, A.C.; Rocha-Santos, T.A.P. Critical overview on the application of sensors and biosensors for clinical analysis. *TrAC Trends Anal. Chem.* **2016**, *85*, 36–60. [CrossRef]

19. Rodbard, D. Continuous glucose monitoring: A review of successes, challenges, and opportunities. *Diabetes Technol. Ther.* **2016**, *18*, S2. [CrossRef]
20. Aydin, E.B.; Aydin, M.; Sezginturk, M.K. Biosensors in drug discovery and drug analysis. *Curr. Anal. Chem.* **2019**, *15*, 467–484. [CrossRef]
21. Chen, Y.; Wang, Z.; Liu, Y.; Wang, X.; Li, Y.; Ma, P.; Gu, B.; Li, H. Recent advances in rapid pathogen detection method based on biosensors. *Eur. J. Clin. Microbiol. Infect. Dis.* **2018**, *37*, 1021–1037. [CrossRef]
22. Cesewski, E.; Johnson, B.N. Electrochemical biosensors for pathogen detection. *Biosens. Bioelectron.* **2020**, *159*, 112214. [CrossRef] [PubMed]
23. Zarei, M. Infectious pathogens meet point-of-care diagnostics. *Biosens. Bioelectron.* **2018**, *106*, 193–203. [CrossRef] [PubMed]
24. Kim, J.; Campbell, A.S.; de Ávila, B.E.-F.; Wang, J. Wearable biosensors for healthcare monitoring. *Nat. Biotechnol.* **2019**, *37*, 389–406. [CrossRef] [PubMed]
25. Gao, W.; Brooks, G.A.; Klonoff, D.C. Wearable physiological systems and technologies for metabolic monitoring. *J. Appl. Phys.* **2018**, *124*, 548–556. [CrossRef]
26. Wu, Q.; Zhang, Y.; Yang, Q.; Yuan, N.; Zhang, W. Review of electrochemical DNA biosensors for detecting food borne pathogens. *Sensors* **2019**, *19*, 4916. [CrossRef]
27. Yu, H.L.L.; Maslova, A.; Hsing, I.-M. Rational design of electrochemical DNA biosensors for point-of-care applications. *Chem. Electro Chem.* **2017**, *4*, 795–805. [CrossRef]
28. Ozer, T.; Geiss, B.J.; Henry, C.S. Review—Chemical and biological sensors for viral detection. *J. Electrochem. Soc.* **2020**, *167*, 037523. [CrossRef]
29. Kokkinos, C.; Economou, A.; Prodromidis, M.I. Electrochemical immunosensors: Critical survey of different architectures and transduction strategies. *TrAC Trends Anal. Chem.* **2016**, *79*, 88–105. [CrossRef]
30. Xiao, X.; Zhu, L.; He, W.; Luo, Y.; Xu, W. Functional nucleic acids tailoring and its application. *TrAC Trends Anal. Chem.* **2019**, *118*, 138–157. [CrossRef]
31. Ilgu, M.; Nilsen-Hamilton, M. Aptamers in analytics. *Analyst* **2016**, *141*, 1551–1568. [CrossRef]
32. Ellington, A.D.; Szostak, J.W. In vitro selection of RNA molecules that bind specific ligands. *Nature* **1990**, *346*, 818–822. [CrossRef] [PubMed]
33. Tuerk, C.; Gold, L. Systematic evolution of ligands by exponential enrichment: RNA ligands to bacteriophage T4 DNA polymerase. *Science* **1990**, *249*, 505–510. [CrossRef] [PubMed]
34. Famulok, M.; Szostak, J.W. In vitro selection of specific ligand-binding nucleic acids. *Angew. Chem.* **1992**, *31*, 979–988. [CrossRef]
35. Ahmed, M.U.; Hossain, M.M.; Tamiya, E. Electrochemical biosensors for medical and food applications. *Electroanalysis* **2008**, *20*, 616–626. [CrossRef]
36. Ríos, Á.; Zougagh, M.; Avila, M. Miniaturization through lab-on-a-chip: Utopia or reality for routine laboratories? A review. *Anal. Chim. Acta* **2012**, *740*, 1–11. [CrossRef]
37. Maduraiveeran, G.; Sasidharan, M.; Ganesan, M. Electrochemical sensor and biosensor platforms based on advanced nanomaterials for biological and biomedical applications. *Biosens. Bioelectron.* **2018**, *103*, 113–129. [CrossRef]
38. Maduraiveeran, G. Bionanomaterial-based electrochemical biosensing platforms for biomedical applications. *Anal. Methods* **2020**, *12*, 1688–1701. [CrossRef]
39. Dimcheva, N. Nanostructures of noble metals as functional materials in biosensors. *Curr. Opin. Electrochem.* **2020**, *19*, 35–41. [CrossRef]
40. Goud, K.Y.; Reddy, K.K.; Satyanarayana, M.; Kummari, S.; Gobi, K.V. A review on recent developments in optical and electrochemical aptamer-based assays for mycotoxins using advanced nanomaterials. *Microchim. Acta* **2020**, *29*, 187. [CrossRef]
41. Kaur, H.; Shorie, M. Nanomaterial based aptasensors for clinical and environmental diagnostic applications. *Nanoscale Adv.* **2019**, *1*, 2123–2138. [CrossRef]
42. Vasilescu, A.; Hayat, A.; Gáspár, S.; Marty, J.-L. Advantages of carbon nanomaterials in electrochemical aptasensors for food analysis. *Electroanalysis* **2018**, *30*, 2–19. [CrossRef]
43. Sharifi, C.; Vahed, S.Z.; Ahmadian, E.; Dizaj, S.M.; Eftekhari, A.; Khalilov, R.; Ahmadi, M.; Hamidi-Aslh, E.; Labib, M. Detection of pathogenic bacteria via nanomaterials-modified aptasensors. *Biosens. Bioelectron.* **2020**, *150*, 111933. [CrossRef] [PubMed]

44. Tretyakov, Y.D.; Goodilin, E.D. Key trends in basic and application-oriented research on nanomaterials. *Russ. Chem. Rev.* **2009**, *78*, 801–820. [CrossRef]
45. Valcarcel, M.; Cardenas, S.; Simonet, B.M.; Moliner-Martinez, Y.; Lucena, R. Carbon nanostructures as sorbent materials in analytical processes. *TrAC Trends Anal. Chem.* **2008**, *27*, 34–43. [CrossRef]
46. Sarapuu, A.; Kibena-Põldsepp, E.; Borghei, M.; Tammeveski, K. Electrocatalysis of oxygen reduction on heteroatom-doped nanocarbons and transition metal–nitrogen–carbon catalysts for alkaline membrane fuel cells. *J. Mater. Chem. A* **2018**, *6*, 776–804. [CrossRef]
47. Pieta, I.S.; Rathi, A.; Pieta, P.; Nowakowski, R.; Hołdynski, M.; Pisarek, M.; Kaminska, A.; Gawande, M.; Zboril, R. Electrocatalytic methanol oxidation over Cu, Ni and bimetallic Cu-Ni nanoparticles supported on graphitic carbon nitride. *Appl. Catal. B* **2019**, *244*, 272–283. [CrossRef]
48. Hu, C.; Dai, L. Doping of carbon materials for metal-free electrocatalysis. *Adv. Mater.* **2019**, *31*, 1804672. [CrossRef]
49. Neto, C.A.H.; Guinea, F.; Peres, N.M.R.; Novoselov, K.S.; Geim, A.K. The electronic properties of graphene. *Rev. Mod. Phys.* **2009**, *81*, 109–162. [CrossRef]
50. Novoselov, K.S.; Geim, A.K.; Morozov, S.V.; Jiang, D.; Zhang, Y.; Dubonos, S.V.; Grigorieva, I.V.; Firsov, A.A. Electric field effect in atomically thin carbon films. *Science* **2004**, *306*, 666–669. [CrossRef]
51. Bonaccorso, F.; Colombo, L.; Yu, G.; Stoller, M.; Tozzini, V.; Ferrari, A.C.; Ruoff, R.S.; Pellegrini, V. 2D materials. Graphene, related two-dimensional crystals, and hybrid systems for energy conversion and storage. *Science* **2015**, *347*, 1246501. [CrossRef]
52. Lotya, M.; Hernandez, Y.; King, P.J.; Smith, R.J.; Nicolosi, V.; Karlsson, L.S.; Blighe, F.M.; De, S.; Wang, Z.; McGovern, I.T.; et al. Liquid phase production of graphene by exfoliation of graphite in surfactant/water solutions. *J. Am. Chem. Soc.* **2009**, *131*, 3611–3620. [CrossRef] [PubMed]
53. Tran-Van, A.F.; Wegner, H.A. Strategies in organic synthesis for condensed arenes, coronene, and graphene. *Top. Curr. Chem.* **2013**, *349*, 121–157. [CrossRef]
54. Zhang, Y.; Zhang, L.; Zhou, C. Review of chemical vapor deposition of graphene and related applications. *Acc. Chem. Res.* **2013**, *46*, 2329–2339. [CrossRef] [PubMed]
55. Stankovich, S.; Dikin, D.A.; Piner, R.D.; Kohlhaas, K.A.; Kleinhammes, A.; Jia, Y.; Wu, Y.; Nguyen, S.B.T.; Ruoff, R.S. Synthesis of graphene-based nanosheets via chemical reduction of exfoliated graphite oxide. *Carbon* **2007**, *45*, 1558–1565. [CrossRef]
56. McAllister, M.J.; Li, J.-L.; Adamson, D.H.; Schniepp, H.C.; Abdala, A.A.; Liu, J.; Herrera-Alonso, M.; Milius, D.L.; Car, R.; Prud'homme, R.K.; et al. Single sheet functionalized graphene by oxidation and thermal expansion of graphite. *Chem. Mater.* **2007**, *19*, 4396–4404. [CrossRef]
57. Xu, S.; Duo, H.; Zheng, C.; Zhao, S.; Song, S.; Simon, G. Novel approach to fabrication of DNA biosensor based on a carboxylated graphene oxide decorated with Fe_3O_4 NPs for the detection of typhoidal salmonella. *Int. J. Electrochem. Sci.* **2019**, *14*, 1248–1269. [CrossRef]
58. Chen, S.-L.; Chen, C.-Y.; Hsieh, J.C.-H.; Yu, Z.-Y.; Cheng, S.-J.; Hsieh, K.Y.; Yang, J.-W.; Kumar, P.V.; Lin, S.-F.; Chen, G.-Y. Graphene oxide-based biosensors for liquid biopsies in cancer diagnosis. *Nanomaterials* **2019**, *9*, 1725. [CrossRef]
59. Rowley-Neale, S.J.; Randviir, E.P.; Dena, A.S.A.; Banks, C.E. An overview of recent applications of reduced graphene oxide as a basis of electroanalytical sensing platforms. *Appl. Mater. Today* **2018**, *10*, 218–226. [CrossRef]
60. Hatamluyi, B.; Es'haghi, Z. A layer-by-layer sensing architecture based on dendrimer and ionic liquid supported reduced graphene oxide for simultaneous hollow-fiber solid phase microextraction and electrochemical determination of anti-cancer drug imatinib in biological samples. *J. Electroanal. Chem.* **2017**, *801*, 439–449. [CrossRef]
61. Zhang, J.; Dai, L. Nitrogen, phosphorus, and fluorine tri-doped graphene as a multifunctional catalyst for self-powered electrochemical water splitting. *Angew. Chem.* **2016**, *55*, 13296–13300. [CrossRef]
62. Wang, G.; Ji, Y.; Lei, Y.; Wang, Y.; Wang, Y.; Li, Y.; Wang, S. Pyridinic-N-dominated doped defective graphene as a superior oxygen electrocatalyst for ultrahigh-energy-density Zn–air batteries. *ACS Energy Lett.* **2018**, *3*, 1183–1191. [CrossRef]
63. Chen, L.; Han, J.; Ito, U.; Fujita, T.; Huang, G.; Hu, K.; Hirata, A.; Watanabe, K.; Chen, M. Heavily doped and highly conductive hierarchical nanoporous graphene for electrochemical hydrogen production. *Angew. Chem.* **2018**, *130*, 13486–13491. [CrossRef]

64. Zhou, F.; Huang, H.; Xiao, C.; Zheng, S.; Shi, X.; Qin, J.; Fu, Q.; Bao, X.; Feng, X.; Müllen, K.; et al. Electrochemically scalable production of fluorine-modified graphene for flexible and high-energy ionogel-based microsupercapacitors. *J. Am. Chem. Soc.* **2018**, *140*, 8198–8205. [CrossRef] [PubMed]
65. Zhang, X.; Gao, J.; Xiao, Y.; Wang, J.; Sun, G.; Zhao, Y.; Qu, L. Regulation of 2D graphene materials for electrocatalysis. *Chem. Eur. J.* **2020**, *15*, 2271–2281. [CrossRef] [PubMed]
66. Cohen, M.L. Nanotubes, nanoscience, and nanotechnology. *Mater. Sci. Eng. C* **2001**, *15*, 1–11. [CrossRef]
67. Kim, S.N.; Rusling, J.F.; Papadimitrakopoulos, F. Carbon nanotubes for electronic and electrochemical detection of biomolecules. *Adv. Mater.* **2007**, *19*, 3214–3228. [CrossRef]
68. Cinke, M.; Li, J.; Chen, B.; Cassell, A.; Delzeit, L.; Han, J.; Meyyappan, M. Pore structure of raw and purified HiPco single-walled carbon nanotubes. *Chem. Phys. Lett.* **2002**, *365*, 69–74. [CrossRef]
69. Frackowiak, E.; Delpeux, S.; Jurewicz, K.; Szostak, K.; Cazorla-Amoros, D.; Béguin, F. Enhanced capacitance of carbon nanotubes through chemical activation. *Chem. Phys. Lett.* **2002**, *336*, 35–41. [CrossRef]
70. Arora, N.; Sharma, N.N. Arc discharge synthesis of carbon nanotubes: Comprehensive review. *Diam. Rel. Mater.* **2014**, *50*, 135–150. [CrossRef]
71. Kuo, T.F.; Chi, C.C.; Lin, I.N. Synthesis of carbon nanotubes by laser ablation of graphites at room temperature. *Jpn. J. Appl. Phys.* **2001**, *40*, 7147–7150. [CrossRef]
72. Dresselhaus, M.S.; Eklund, P.C. Phonons in carbon nanotubes. *Adv. Phys.* **2000**, *49*, 705–814. [CrossRef]
73. Thorogood, C.A.; Wildgoose, G.G.; Crossley, A.; Jacobs, R.M.J.; Jones, J.H.; Compton, R.G. Differentiating between ortho- and para-quinone surface groups on graphite, glassy carbon, and carbon nanotubes using organic and inorganic voltammetric and X-ray photoelectron spectroscopy labels. *Chem. Mater.* **2007**, *19*, 4964–4974. [CrossRef]
74. Patil, I.M.; Reddy, V.; Lokanathan, M.; Kakade, B. Nitrogen and sulphur co-doped multiwalled carbon nanotubes as an efficient electrocatalyst for improved oxygen electroreduction. *Appl. Surf. Sci.* **2018**, *449*, 697–704. [CrossRef]
75. Song, S.; Zhang, L.; Su, Y.; Lv, Y. Recent advances in graphitic carbon nitride-based chemiluminescence, cataluminescence and electrochemiluminescence. *J. Anal. Test.* **2017**, *1*, 274–290. [CrossRef]
76. Ismael, M.; Wu, Y. A mini-review on the synthesis and structural modification of g-C_3N_4-based materials, and their applications in solar energy conversion and environmental remediation. *Sustain. Energy Fuels* **2019**, *3*, 2907–2925. [CrossRef]
77. Cheng, C.; Huang, Y.; Tian, X.; Zheng, B.; Li, Y.; Yuanm, H.; Xiao, D.; Xie, S.; Choim, M.M.F. Electrogenerated chemiluminescence behavior of graphite-like carbon nitride and its application in selective sensing Cu^{2+}. *Anal. Chem.* **2012**, *84*, 4754–4759. [CrossRef]
78. Dong, G.; Zhang, Y.; Pan, Q.; Qiu, J. A fantastic graphitic carbon nitride (g-C_3N_4) material: Electronic structure, photocatalytic and photoelectronic properties. *J. Photochem. Photobiol. C* **2014**, *20*, 33–50. [CrossRef]
79. Jin, H.; Guo, C.; Liu, X.; Liu, J.; Vasileff, A.; Jiao, Y.; Zheng, Y.; Qiao, S.-Z. Emerging two-dimensional nanomaterials for electrocatalysis. *Chem. Rev.* **2018**, *118*, 6337–6408. [CrossRef]
80. Hindermann-Bischoff, M.; Ehrburger-Dolle, F. Electrical conductivity of carbon black–polyethylene composites: Experimental evidence of the change of cluster connectivity in the PTC effect. *Carbon* **2001**, *39*, 375–382. [CrossRef]
81. Chowdhury, Z.Z.; Sagadevan, S.; Johan, R.B.; Shah, S.T.; Adebesi, A.; Md, S.I.; Rafique, R.F. A review on electrochemically modified carbon nanotubes (CNTs) membrane for desalination and purification of water. *Mater. Res. Express* **2018**, *5*, 102001. [CrossRef]
82. Arduini, F.; Cinti, S.; Mazzaracchio, V.; Scognamiglio, V.; Amine, A.; Moscone, D. Carbon black as an outstanding and affordable nanomaterial for electrochemical (bio)sensor design. *Biosens. Bioelectron.* **2020**, *156*, 112033. [CrossRef] [PubMed]
83. Shuai, H.-L.; Huang, K.-J.; Chen, Y.-X. A layered tungsten disulfide/acetylene black composite based DNA biosensing platform coupled with hybridization chain reaction for signal amplification. *J. Mater. Chem. B* **2016**, *4*, 1186–1196. [CrossRef] [PubMed]
84. Lee, D.; Kim, Y.H.; Park, S. Enzyme electrode platform using methyl viologen electrochemically immobilized on carbon materials. *J. Electrochem. Soc.* **2016**, *163*, G93–G98. [CrossRef]
85. Ramsden, J.J. Carbon based nanomaterials and devices. In *Nanotechnology*, 1st ed.; Ramsden, J., Ed.; Elsevier: Cambridge, MA, USA, 2011; pp. 189–197. [CrossRef]

86. Alekseyev, N.I.; Dyuzhev, G.A. Fullerenee formation in an arc discharge. *Carbon* **2003**, *41*, 1343–1348. [CrossRef]
87. Kozlov, B.N.; Kirillov, S.N.; Mamyrin, B.A. Formation of fullerenes in laser ablation of graphite in a vacuum. *Proc. SPIE* **1997**, 3093. [CrossRef]
88. Fink, D.; Chadderton, L.T.; Vacik, J.; Hnatowicz, V.; Zawislak, F.C.; Behar, M.; Grande, D.L. Damage and sputtering of fullerene by low energy medium and heavy ions. *Nucl. Instr. Meth. Phys. Res. B* **1996**, *113*, 244–247. [CrossRef]
89. Yáñez-Sedeño, P.; Campuzano, S.; Pingarrón, J.M. Fullerenes in electrochemical catalytic and affinity biosensing: A review. *J. Carbon. Res.* **2017**, *3*, 21. [CrossRef]
90. Gergeroglu, H.; Yildirim, S.; Ebeoglugil, M.F. Nano-carbons in biosensor applications: An overview of carbon nanotubes (CNTs) and fullerenes (C60). *SN Appl. Sci.* **2020**, *2*, 603. [CrossRef]
91. Kumar, Y.R.; Deshmukh, K.; Sadasivuni, K.K.; Pasha, S.K.K. Graphene quantum dot based materials for sensing, bio-imaging and energy storage applications: A review. *RSC Adv.* **2020**, *10*, 23861. [CrossRef]
92. Liu, M.L.; Chen, B.B.; Li, C.M.; Huang, C.Z. Carbon dots: Synthesis, formation mechanism, fluorescence origin and sensing applications. *Green Chem.* **2019**, *21*, 449–471. [CrossRef]
93. Tuerhong, M.; Xu, Y.; Yin, X.-B. Review on carbon dots and their applications. *Chin. J. Anal. Chem.* **2017**, *45*, 139–150. [CrossRef]
94. Sciortino, A.; Cannizzo, A.; Messina, F. Carbon nanodots: A review—From the current understanding of the fundamental photophysics to the full control of the optical response. *C J. Carbon Res.* **2018**, *4*, 67. [CrossRef]
95. Tajik, S.; Dourandish, Z.; Zhang, K.; Beitollahi, H.; Le, O.V.; Jang, H.W.; Shokouhimehr, M. Carbon and graphene quantum dots: A review on syntheses, characterization, biological and sensing applications for neurotransmitter determination. *RSC Adv.* **2020**, *10*, 15406–15429. [CrossRef]
96. He, M.; Guo, X.; Huang, J.; Shen, H.; Zeng, Q.; Wang, L. Mass production of tunable multicolor graphene quantum dots from an energy resource of coke by a one step electrochemical exfoliation. *Carbon* **2018**, *140*, 508–520. [CrossRef]
97. Viculis, L.M.; Mack, J.J.; Mayer, O.M.; Hahn, H.T.; Kaner, R.B. Intercalation and exfoliation routes to graphite nanoplatelets. *J. Mater. Chem.* **2005**, *15*, 974–978. [CrossRef]
98. Hong, G.L.; Zhao, H.L.; Deng, H.H.; Yang, H.J.; Peng, H.P.; Liu, Y.H.; Chen, W. Fabrication of ultra-small monolayer graphene quantum dots by pyrolysis of trisodium citrate for fluorescent cell imaging. *Int. J. Nanomed.* **2018**, *13*, 4807–4815. [CrossRef]
99. Titirici, M.M.; Antonietti, M. Chemistry and materials options of sustainable carbon materials made by hydrothermal carbonization. *Chem. Soc. Rev.* **2010**, *39*, 103–116. [CrossRef]
100. Baccile, N.; Antonietti, M.; Titirici, M.-M. One-step hydrothermal synthesis of nitrogen-doped nanocarbons: Albumin directing the carbonization of glucose. *Chem. Sustain. Chem.* **2010**, *3*, 246–253. [CrossRef]
101. Cui, X.; Antonietti, M.; Yu, S.-H. Structural effects of iron oxide nanoparticles and iron ions on the hydrothermal carbonization of starch and rice carbohydrates. *Small* **2006**, *2*, 756–759. [CrossRef]
102. Ding, X.; Niu, Y.; Zhang, G.; Xu, Y.; Li, J. Electrochemistry in carbon-based quantum dots. *Chem. Asian J.* **2020**, *15*, 1214–1224. [CrossRef]
103. Grabowska, I.; Sharma, N.; Vasilescu, A.; Iancu, M.; Badea, G.; Boukherroub, R.; Ogale, S.; Szunerits, S. Electrochemical aptamer-based biosensors for the detection of cardiac biomarkers. *ACS Omega* **2018**, *3*, 12010–12018. [CrossRef] [PubMed]
104. Kong, T.; Zhou, R.; Zhang, Y.; Hao, L.; Cai, X.; Zhu, B. AS1411 aptamer modified carbon dots via polyethylenimine-assisted strategy for efficient targeted cancer cell imaging. *Cell Prolif.* **2020**, *53*, 312713. [CrossRef] [PubMed]
105. Kulikova, T.N.; Porfireva, A.V.; Evtugyn, G.A.; Hianik, T. Electrochemical aptasensor with layer-by-layer deposited polyaniline for aflatoxin M1 voltammetric determination. *Electroanalysis* **2019**, *31*, 1913–1924. [CrossRef]
106. Palchetti, I.; Mascini, M. Electrochemical adsorption technique for immobilization of single-stranded oligonucleotides onto carbon screen-printed electrodes. In *Immobilisation of DNA on Chips II. Topics in Current Chemistry*; Wittmann, C., Ed.; Springer: Berlin/Heidelberg, Germany, 2006; p. 261. [CrossRef]
107. Du, Y.; Chen, C.; Li, B.; Zhou, M.; Wang, E.; Dong, S. Layer-by-layer electrochemical biosensor with aptamer-appended activepolyelectrolyte multilayer for sensitive protein determination. *Biosens. Bioelectron.* **2010**, *25*, 1902–1907. [CrossRef]

108. Kim, P.J.P.; Lee, B.Y.; Hong, S.; Sim, S.J. Ultrasensitive carbon nanotube-based biosensors using antibody-binding fragments. *Anal. Biochem.* **2008**, *381*, 193–198. [CrossRef]
109. Zhang, X.; Servos, M.R.; Liu, J. Instantaneous and quantitative functionalization of gold nanoparticles with thiolated DNA using a pH-assisted and surfactant-free route. *J. Am. Chem. Soc.* **2012**, *134*, 7266–7269. [CrossRef]
110. Oberhaus, F.V.; Frense, D.; Beckmann, D. Immobilization techniques for aptamers on gold electrodes for the electrochemical detection of proteins: A review. *Biosensors* **2020**, *10*, 45. [CrossRef]
111. Cammarata, C.R.; Hughes, M.E.; Ofner, C.M., III. Carbodiimide induced cross-linking, ligand addition, and degradation in gelatin. *Mol. Pharm.* **2015**, *12*, 783–793. [CrossRef]
112. Baranton, S.; Bélanger, D. Electrochemical derivatization of carbon surface by reduction of in situ generated diazonium cations. *J. Phys. Chem. B* **2005**, *109*, 24401–24410. [CrossRef]
113. Mishra, R.K.; Hayat, A.; Catanante, G.; Ocaña, C.; Marty, J.-L. A label free aptasensor for Ochratoxin A detection in cocoa beans: An application to chocolate industries. *Anal. Chim. Acta* **2015**, *889*, 106–112. [CrossRef]
114. Witt, M.; Walter, J.-G.; Stahl, F. Aptamer microarrays—Current status and future prospects. *Microarrays* **2015**, *4*, 115–132. [CrossRef] [PubMed]
115. Balamurugan, S.; Obubuafo, A.; McCarley, R.L.; Soper, S.A.; Spivak, D.A. Effect of linker structure on surface density of aptamer monolayers and their corresponding protein binding efficiency. *Anal. Chem.* **2008**, *80*, 9630–9634. [CrossRef] [PubMed]
116. Dupont-Filliard, A.; Billon, M.; Livache, T.; Guillerez, S. Biotin/avidin system for the generation of fully renewable DNA sensor based on biotinylated polypyrrole film. *Anal. Chim. Acta* **2004**, *515*, 271–277. [CrossRef]
117. Baghbaderani, S.S.; Noorbakhsh, A. Novel chitosan-Nafion composite for fabrication of highly sensitive impedimetric and colorimetric As(III) aptasensor. *Biosens. Bioelectron.* **2019**, *131*, 1–8. [CrossRef] [PubMed]
118. Tahmasebi, F.; Noorbakhsh, A. Sensitive electrochemical prostate specific antigen aptasensor: Effect of carboxylic acid functionalized carbon nanotube and glutaraldehyde linker. *Electroanalysis* **2016**, *28*, 1134–1145. [CrossRef]
119. Hummers, W.S.; Offeman, R.E.W. Preparation of graphitic oxide. *J. Am. Chem. Soc.* **1958**, *80*, 1339. [CrossRef]
120. Yu, H.; Zhang, B.; Bulin, C.; Li, R.; Xing, R. High-efficient synthesis of graphene oxide based on improved Hummers method. *Sci. Rep.* **2016**, *6*, 36143. [CrossRef]
121. Pourmadadi, M.; Shayeh, J.; Omidi, M.; Yazdian, F.; Alebouyeh, M.; Tayebi, L. A glassy carbon electrode modified with reduced graphene oxide and gold nanoparticles for electrochemical aptasensing of lipopolysaccharides from Escherichia coli bacteria. *Microchim. Acta* **2019**, *186*, 787. [CrossRef]
122. Rezaei, B.; Jamei, H.R.; Ensafi, A.A. An ultrasensitive and selective electrochemical aptasensor based on rGO-MWCNTs/chitosan/carbon quantum dot for the detection of lysozyme. *Biosens. Bioelectron.* **2018**, *115*, 37–44. [CrossRef]
123. Fu, J.; An, X.; Yao, Y.; Guo, Y.; Sun, X. Electrochemical aptasensor based on one step co-electrodeposition of aptamer and GO-CuNPs nanocomposite for organophosphorus pesticide detection. *Sens. Actuators B Chem.* **2019**, *287*, 503–509. [CrossRef]
124. Yang, S.; Teng, Y.; Cao, Q.; Bai, C.; Fang, Z.; Xu, W. Electrochemical sensor based on molecularly imprinted polymer-aptamer hybrid receptor for voltammetric detection of thrombin. *J. Electrochem. Soc.* **2019**, *166*, B23–B28. [CrossRef]
125. Yang, S.; Yang, J.; Cao, Q.; Zheng, Y.; Bai, C.; Teng, Y.; Xu, W. A molecularly imprinted polythionine-modified electrode based on a graphene-gold nanoparticle composite (MIP/AuNPs/rGO/GCE) for the determination of thrombin. *Int. J. Electrochem. Sci.* **2018**, *13*, 9333–9345. [CrossRef]
126. Gao, S.; Zheng, X.; Jiao, B.; Wang, L. Post-SELEX optimization of aptamers. *Anal. Bioanal. Chem.* **2016**, *408*, 4567–4573. [CrossRef] [PubMed]
127. Bai, C.; Lu, Z.; Jiang, H.; Yang, Z.; Liu, X.; Ding, H.; Li, H.; Dong, J.; Huang, A.; Fang, T.; et al. Aptamer selection and application in multivalent binding-based electrical impedance detection of inactivated H1N1 virus. *Biosens. Bioelectron.* **2018**, *110*, 162–167. [CrossRef] [PubMed]
128. Guo, S.; Wen, J.; Song, L.; Qu, J.; He, W.; Liu, S. One-step fabrication and electromagnetic wave absorption of graphene/Ag@polyaniline ternary nanocomposites. *Nanotechnology* **2020**, *31*, 225606. [CrossRef]

129. Romero, A.; Lavín-López, M.P.; de la Osa, A.R.; Ordoñez, S.; de Lucas-Consuegra, A.; Valverde, J.L.; Patón, A. Different strategies to simultaneously N-doping and reduce graphene oxide for electrocatalytic applications. *J. Electroanal. Chem.* **2020**, *857*, 113695. [CrossRef]
130. Lazar, J.; Schnelting, C.; Slavcheva, E.; Schnakenberg, U. Hampering of the stability of gold electrodes by ferri-/ferrocyanide redox couple electrolytes during electrochemical impedance spectroscopy. *Anal. Chem.* **2016**, *88*, 682–687. [CrossRef]
131. Roxo, C.; Kotkowiak, W.; Pasternak, A. G-Quadruplex-forming aptamers—Characteristics, applications, and perspectives. *Molecules* **2019**, *24*, 3781. [CrossRef]
132. Ma, D.-L.; Zhang, Z.; Wang, M.; Lu, L.; Zhong, H.-J.; Leung, C.-H. Recent developments in G-quadruplex probes. *Chem. Biol.* **2015**, *22*, 812–828. [CrossRef]
133. Chai, H.; Ma, X.; Meng, F.; Mei, Q.; Tang, Y.; Miao, P. Electrochemical aptasensor based on a potassium ion-triggered DNA conformation transition and self-assembly on an electrode. *New J. Chem.* **2019**, *43*, 7928–7931. [CrossRef]
134. Lubin, A.A.; Plaxco, K.W. Folding-based electrochemical biosensors: The case for responsive nucleic acid architectures. *Acc. Chem. Res.* **2010**, *43*, 496–505. [CrossRef] [PubMed]
135. Li, H.; Ding, S.; Wang, W.; Lv, Q.; Wang, Z.; Bai, H.; Zhang, Q. Voltammetric aptasensor for bisphenol A based on double signal amplification via gold-coated multiwalled carbon nanotubes and an ssDNA-dye complex. *Microchim. Acta* **2019**, *186*, 860. [CrossRef] [PubMed]
136. Mashhadizadeh, M.H.; Naser, N.; Mehrgardi, M.A. A digoxin electrochemical aptasensor using Ag nanoparticle decorated graphene oxide. *Anal. Methods* **2016**, *8*, 7247–7253. [CrossRef]
137. He, B.; Yan, X. An amperometric zearalenone aptasensor based on signal amplification by using a composite prepared from porous platinum nanotubes, gold nanoparticles and thionine-labelled graphene oxide. *Microchim. Acta* **2019**, *186*, 383. [CrossRef] [PubMed]
138. He, B.; Li, M.; Li, M. Electrochemical determination of sulfamethazine using a gold electrode modified with multi-walled carbon nanotubes, graphene oxide nanoribbons and branched aptamers. *Microchim. Acta* **2020**, *187*, 274. [CrossRef] [PubMed]
139. Zhu, X.; Kou, F.; Xu, X.; Han, Y.; Yang, G.; Huang, X.; Chen, W.; Chie, Y.; Lin, Z. Label-free ochratoxin A electrochemical aptasensor based on target-induced noncovalent assembly of peroxidase-like graphitic carbon nitride nanosheet. *Sens. Actuators B Chem.* **2018**, *270*, 263–269. [CrossRef]
140. You, H.; Bai, L.; Yuan, Y.; Zhou, J.; Bai, Y.; Mu, Z. An amperometric aptasensor for ultrasensitive detection of sulfadimethoxine based on exonuclease-assisted target recycling and new signal tracer for amplification. *Biosens. Bioelectron.* **2018**, *117*, 706–712. [CrossRef]
141. HJornbeck, P. Enzyme-Linked Immunosorbent Assays. *Curr. Protoc. Immun.* **1992**, *1*. [CrossRef]
142. Ferrua, B.; Vincent, C.; Revillard, J.P.; Pettazzi, G.; Maiolini, T.; Viot, G.; Masseyeff, R. A sandwich method of enzyme immunoassay. *III. Assay for human beta-2 microglobulin compared with radioimmunoassay. J. Immun. Methods* **1980**, *36*, 149–158. [CrossRef]
143. Jarczewska, M.; Malinowska, E. The application of antibody–aptamer hybrid biosensors in clinical diagnostics and environmental analysis. *Anal. Methods* **2020**, *12*, 3183–3199. [CrossRef]
144. Song, Q.; Wang, R.; Sun, F.; Chen, H.; Wang, Z.; Na, N.; Ouyang, J. A nuclease-assisted label-free aptasensor for fluorescence turn-on detection of ATP based on the in situ formation of copper nanoparticles. *Biosens. Bioelectron.* **2017**, *87*, 760–763. [CrossRef] [PubMed]
145. Wang, Y.-H.; Chen, Y.-X.; Wu, X.; Huang, K.-J. Electrochemical biosensor based on Se-doped MWCNTs-graphene and Y- shaped DNA-aided target-triggered amplification strategy. *Colloids Surf. B* **2018**, *172*, 407–413. [CrossRef] [PubMed]
146. Majd, S.M.; Salimi, A. Ultrasensitive flexible FET-type aptasensor for CA 125 cancer marker detection based on carboxylated multiwalled carbon nanotubes immobilized onto reduced graphene oxide film. *Anal. Chim. Acta* **2018**, *1000*, 273–282. [CrossRef]
147. Gao, N.; Gao, T.; Yang, X.; Dai, X.; Zhou, W.; Zhang, A.; Lieber, C.M. Specific detection of biomolecules in physiological solutions using graphene transistor biosensors. *Proc. Nalt. Acad. Sci. USA* **2016**, *113*, 14633–14638. [CrossRef] [PubMed]
148. Khung, Y.L.; Narducci, D. Synergizing nucleic acid aptamers with 1-dimensional nanostructures as label-free field-effect transistor biosensors. *Biosens. Bioelectron.* **2013**, *50*, 278–293. [CrossRef] [PubMed]

149. Derikvandi, Z.; Abbasi, A.R.; Roushani, M.; Derikvand, Z.; Azadbakht, A. Design of ultrasensitive bisphenol A aptamer based on platinum nanoparticles loading to polyethyleneimine-functionalized carbon nanotubes. *Anal. Biochem.* **2016**, *512*, 47–57. [CrossRef] [PubMed]
150. Azadbakht, A.; Abbasi, A.R. Engineering an aptamer-based recognition sensor for electrochemical opium alkaloid biosensing. *J. Mater. Sci.* **2019**, *30*, 3432–3442. [CrossRef]
151. Ghanbari, K.; Roushani, M. A nanohybrid probe based on double recognition of an aptamer MIP grafted onto a MWCNTs-Chit nanocomposite for sensing hepatitis C virus core antigen. *Sens. Actuators B Chem.* **2018**, *258*, 1066–1071. [CrossRef]
152. Nazari, M.; Kashanian, S.; Rafipour, R.; Omidfar, K. Biosensor design using an electroactive label-based aptamer to detect bisphenol A in serum samples. *J. Biosci.* **2019**, *44*, 105. [CrossRef]
153. Baghayeri, M.; Ansari, R.; Nodehi, M.; Razavipanah, I.; Veisi, H. Label-free electrochemical bisphenol A aptasensor based on designing and fabrication of a magnetic gold nanocomposite. *Electroanalysis* **2018**, *30*, 2160–2166. [CrossRef]
154. Azadbakht, A.; Roushani, M.; Abbasi, A.R.; Derikvand, Z. A novel impedimetric aptasensor, based on functionalized carbon nanotubes and prussian blue as labels. *Anal. Biochem.* **2016**, *512*, 58–69. [CrossRef] [PubMed]
155. Haghshenas, E.; Madrakian, T.; Afkhami, A.; Nabiabad, H.S. An electrochemical ceruloplasmin aptasensor using a glassy carbon electrode modified by diazonium-functionalized multiwalled carbon nanotubes. *J. Iran. Chem. Soc.* **2019**, *16*, 593–602. [CrossRef]
156. Xu, G.; Huo, D.; Hou, C.; Zhao, Y.; Bao, J.; Yang, M.; Fa, H. A regenerative and selective electrochemical aptasensor based on copper oxide nanoflowers-single walled carbon nanotubes nanocomposite for chlorpyrifos detection. *Talanta* **2018**, *178*, 1046–1052. [CrossRef] [PubMed]
157. Hu, X.; Goud, K.Y.; Kumar, V.S.; Catanante, G.; Li, Z.; Zhu, Z.; Marty, J.L. Disposable electrochemical aptasensor based on carbon nanotubes- V_2O_5-chitosan nanocomposite for detection of ciprofloxacin. *Sens. Actuators B Chem.* **2018**, *268*, 278–286. [CrossRef]
158. Shiravand, T.; Azadbakht, A. Impedimetric biosensor based on bimetallic AgPt nanoparticle-decorated carbon nanotubes as highly conductive film surface. *J. Solid State Electrochem.* **2017**, *21*, 1699–1711. [CrossRef]
159. Azadbakht, A.; Roushani, M.; Abbasi, A.R.; Derikvand, Z. Design and characterization of electrochemical dopamine aptamer as convenient and integrated sensing platform. *Anal. Biochem.* **2016**, *507*, 47–57. [CrossRef]
160. Azadbakht, A.; Roushani, M.; Abbasi, A.R.; Menati, S.; Derikvand, Z.A. label-free aptasensor based on polyethyleneimine wrapped carbon nanotubes in situ formed gold nanoparticles as signal probe for highly sensitive detection of dopamine. *Mater. Sci. Eng. C* **2016**, *68*, 585–593. [CrossRef]
161. Beiranvand, S.; Abbasi, A.R.; Roushani, M.; Derikvand, Z.; Azadbakht, A. A simple and label-free aptasensor based on amino group-functionalized gold nanocomposites-Prussian blue/carbon nanotubes as labels for signal amplification. *J. Electroanal. Chem.* **2016**, *776*, 170–179. [CrossRef]
162. Hashkavayi, A.B.; Raoof, J.B.; Ojani, R. Preparation of epirubicin aptasensor using curcumin as hybridization indicator: Competitive binding assay between complementary strand of aptamer and epirubicin. *Electroanalysis* **2018**, *30*, 378–385. [CrossRef]
163. Ming, T.; Wang, Y.; Luo, J.; Liu, J.; Sun, S.; Xing, Y.; Xiao, G.; Jin, H.; Cai, X. Folding paper-based aptasensor platform coated with novel nanoassemblies for instant and highly sensitive detection of 17β-estradiol. *ACS Sens.* **2019**, *4*, 3186–3194. [CrossRef]
164. Liu, X.; Deng, K.; Wang, H.; Li, C.; Zhang, S.; Huang, H. Aptamer based ratiometric electrochemical sensing of 17β-estradiol using an electrode modified with gold nanoparticles, thionine, and multiwalled carbon nanotubes. *Microchim. Acta* **2019**, *186*, 347. [CrossRef] [PubMed]
165. Roushani, M.; Shahdost-fard, F. Covalent attachment of aptamer onto nanocomposite as a high performance electrochemical sensing platform: Fabrication of an ultra-sensitive ibuprofen electrochemical aptasensor. *Mater. Sci. Eng. C* **2016**, *68*, 128–135. [CrossRef] [PubMed]
166. Douaki, A.; Abera, B.D.; Cantarella, G.; Shkodra, B.; Mushtaq, A.; Ibba, P.; Inam, A.S.; Petti, L.; Lugli, P. Flexible screen printed aptasensor for rapid detection of furaneol: A comparison of CNTs and AgNPs effect on aptasensor performance. *Nanomaterials* **2020**, *10*, 1167. [CrossRef] [PubMed]
167. Azadbakht, A.; Abbasi, A.R. Impedimetric aptasensor for kanamycin by using carbon nanotubes modified with $MoSe_2$ nanoflowers and gold nanoparticles as signal amplifiers. *Microchim. Acta* **2019**, *186*, 23. [CrossRef]

168. Kaur, N.; Thakur, H.; Prabhakar, N. Multiwalled carbon nanotubes embedded conducting polymer based electrochemical aptasensor for estimation of malathion. *Microchem. J.* **2019**, *147*, 393–402. [CrossRef]
169. Nawaz, M.A.H.; Rauf, S.; Catanante, G.; Nawaz, M.H.; Nunes, G.; Marty, J.L.; Hayat, A. One step assembly of thin films of carbon nanotubes on screen printed interface for electrochemical aptasensing of breast cancer biomarker. *Sensors* **2016**, *16*, 1651. [CrossRef]
170. Nia, N.G.; Azadbakht, A. Nanostructured aptamer-based sensing platform for highly sensitive recognition of myoglobin. *Microchim. Acta* **2018**, *185*, 333. [CrossRef]
171. Wang, H.; Pan, L.; Liu, Y.; Ye, Y.; Yao, Y. Electrochemical sensing of nitenpyram based on the binary nanohybrid of hydroxylated multiwall carbon nanotubes/single-wall carbon nanohorns. *J. Electroanal. Chem.* **2020**, *862*, 113955. [CrossRef]
172. He, B.; Wang, L.; Dong, X.; Yan, X.; Li, M.; Yan, S.; Yan, D. Aptamer-based thin film gold electrode modified with gold nanoparticles and carboxylated multi-walled carbon nanotubes for detecting oxytetracycline in chicken samples. *Food Chem.* **2019**, *300*, 125179. [CrossRef]
173. Zheng, H.Y.; Alsager, O.A.; Zhu, B.; Travas-Sejdic, J.; Hodgkiss, J.M.; Plank, N.O.V. Electrostatic gating in carbon nanotube aptasensors. *Nanoscale* **2016**, *8*, 13659–13668. [CrossRef]
174. Zhang, H.; Sun, J.; Cheng, S.; Liu, H.; Li, F.; Guo, Y.; Sun, X. A dual-amplification electrochemical aptasensor for profenofos detection. *J. Electrochem. Soc.* **2020**, *167*, 027515. [CrossRef]
175. Hasan, M.R.; Pulingam, T.; Appaturi, J.N.; Zifruddin, A.N.; Teh, S.J.; Lim, T.W.; Ibrahim, F.; Leo, B.F.; Thong, K.L. Carbon nanotube-based aptasensor for sensitive electrochemical detection of whole-cell Salmonella. *Anal. Biochem.* **2018**, *554*, 34–43. [CrossRef] [PubMed]
176. Hou, L.; Jiang, L.; Song, Y.; Ding, Y.; Zhang, J.; Wu, X.; Tang, D. Amperometric aptasensor for saxitoxin sing a gold electrode modified with carbon nanotubes on a self-assembled monolayer, and methylene blue as an electrochemical indicator probe. *Microchim. Acta* **2016**, *183*, 1971–1980. [CrossRef]
177. Aghajari, R.; Azadbakht, A. Amplified detection of streptomycin using aptamer-conjugated palladium nanoparticles decorated on chitosan-carbon nanotube. *Anal. Biochem.* **2018**, *547*, 57–65. [CrossRef] [PubMed]
178. Yin, Y.; Qin, X.; Wang, Q.; Yin, Y. A novel electrochemical aptasensor for sensitive detection of streptomycin based on gold nanoparticle-functionalized magnetic multi-walled carbon nanotubes and nanoporous PtTi alloy. *RSC Adv.* **2016**, *6*, 39401–39408. [CrossRef]
179. Yin, J.; Guo, W.; Qin, X.; Pei, M.; Wang, L.; Ding, F. A regular "signal attenuation" electrochemical aptasensor for highly sensitive detection of streptomycin. *New J. Chem.* **2016**, *40*, 9711–9718. [CrossRef]
180. He, B.; Du, G. Novel electrochemical aptasensor for ultrasensitive detection of sulfadimidine based on covalently linked multi-walled carbon nanotubes and in situ synthesized gold nanoparticle composites. *Anal. Bioanal. Chem.* **2018**, *410*, 2901–2910. [CrossRef]
181. He, B.-S.; Yan, S. Electrochemical aptasensor based on aptamer complimentary strand conjugate and thionine for sensitive detection of tetracycline with multiwalled carbon nanotubes and gold nanoparticles amplification. *Anal. Methods* **2018**, *10*, 783–790. [CrossRef]
182. Benvidi, A.; Yazdanparast, S.; Rezaeinasab, M.; Tezerjani, M.D.; Abbasi, S. Designing and fabrication of a novel sensitive electrochemical aptasensor based on poly (L-glutamic acid)/MWCNTs modified glassy carbon electrode for determination of tetracycline. *J. Electroanal. Chem.* **2018**, *808*, 311–320. [CrossRef]
183. Hou, W.; Shi, Z.; Guo, Y.; Sun, X.; Wang, X. An interdigital array microelectrode aptasensor based on multi-walled carbon nanotubes for detection of tetracycline. *Bioprocess Biosyst. Eng.* **2017**, *40*, 1419–1425. [CrossRef]
184. Heydari-Bafrooei, E.; Amini, M.; Ardakani, M.H. An electrochemical aptasensor based on TiO_2/MWCNT and a novel synthesized Schiff base nanocomposite for the ultrasensitive detection of thrombin. *Biosens. Bioelectron.* **2016**, *85*, 828–836. [CrossRef] [PubMed]
185. Su, Z.; Xu, X.; Xu, H.; Zhang, Y.; Li, C.; Ma, Y.; Song, D.; Xie, Q. Amperometric thrombin aptasensor using a glassy carbon electrode modified with polyaniline and multiwalled carbon nanotubes tethered with a thiolated aptamer. *Microchim. Acta* **2017**, *184*, 1677–1682. [CrossRef]
186. Hashkavayi, A.B.; Raoof, J.B. Ultrasensitive and reusable electrochemical aptasensor for detection of tryptophan using of $[Fe(bpy)_3](p\text{-}CH_3C_6H_4SO_2)_2$ as an electroactive indicator. *J. Pharm. Biomed. Anal.* **2019**, *163*, 180–187. [CrossRef] [PubMed]

187. Majidi, M.R.; Karami, P.; Johari-Aharc, M.; Omidi, Y. Direct detection of tryptophan for rapid diagnosis of cancer cell metastasis competence by an ultra- sensitive and highly selective electrochemical biosensor. *Anal. Methods* **2016**, *8*, 7910–7919. [CrossRef]
188. Majidi, M.R.; Omidi, Y.; Karami, P.; Johari-Ahar, M. Reusable potentiometric screen-printed sensor and label-free aptasensor with pseudo-reference electrode for determination of tryptophan in the presence of tyrosine. *Talanta* **2016**, *150*, 425–433. [CrossRef]
189. Yarahmadi, S.; Azadbakht, A.; Derikvand, R.M. Hybrid synthetic receptor composed of molecularly imprinted polydopamine and aptamers for impedimetric biosensing of urea. *Microchim. Acta* **2019**, *186*, 71. [CrossRef]
190. Ma, L.; Bai, L.; Zhao, M.; Zhou, J.; Chen, Y.; Mu, Z. An electrochemical aptasensor for highly sensitive detection of zearalenone based on PEI-MoS_2-MWCNTs nanocomposite for signal enhancement. *Anal. Chim. Acta* **2019**, *1060*, 71–78. [CrossRef]
191. Dan, X.; Ruiyi, L.; Zaijun, L.; Haiyan, Z.; Zhiguo, G.; Guangli, W. Facile strategy for synthesis of silver-graphene hybrid with controllable size and excellent dispersion for ultrasensitive electrochemical detection of acetamiprid. *Appl. Surf. Sci* **2020**, *512*, 145628. [CrossRef]
192. Lin, T.; Shen, Y. Fabricating electrochemical aptasensors for detecting aflatoxin B1 via layer-by-layer self-assembly. *J. Electroanal. Chem.* **2020**, *870*, 114247. [CrossRef]
193. Ge, L.; Wang, W.; Sun, X.; Hou, T.; Li, F. Affinity-mediated homogeneous electrochemical aptasensor on a graphene platform for ultrasensitive biomolecule detection via exonuclease-assisted target-analog recycling amplification. *Anal. Chem.* **2016**, *88*, 2212–2219. [CrossRef]
194. Shekari, Z.; Zare, H.R.; Falahati, A. Electrochemical sandwich aptasensor for the carcinoembryonic antigen using graphene quantum dots, gold nanoparticles and nitrogen doped graphene modified electrode and exploiting the peroxidase-mimicking activity of a G-quadruplex DNAzyme. *Microchim. Acta* **2019**, *186*, 530. [CrossRef] [PubMed]
195. Wei, B.; Zhong, H.; Wang, L.; Liu, Y.; Xu, Y.; Zhang, J.; Xu, C.; He, L.; Wang, H. Facile preparation of a collagen-graphene oxide composite: A sensitive and robust electrochemical aptasensor for determining dopamine in biological samples. *Intern. J. Biol. Macromol.* **2019**, *135*, 400–406. [CrossRef] [PubMed]
196. Jin, H.; Zhao, C.; Gui, R.; Gao, X.; Wang, Z. Reduced graphene oxide/nile blue/gold nanoparticles complex-modified glassy carbon electrode used as a sensitive and label-free aptasensor for ratiometric electrochemical sensing of dopamine. *Anal. Chim. Acta* **2018**, *1025*, 154–162. [CrossRef] [PubMed]
197. Gupta, P.; Bharti, A.; Kaur, N.; Singh, S.; Prabhakar, N. An electrochemical aptasensor based on gold nanoparticles and graphene oxide doped poly(3,4-ethylenedioxythiophene) nanocomposite for detection of MUC1. *J. Electroanal. Chem.* **2018**, *813*, 102–108. [CrossRef]
198. Sharma, A.; Bhardwaj, J.; Jang, J. Label-free, highly sensitive electrochemical aptasensors using polymer-modified reduced graphene oxide for cardiac biomarker detection. *ACS Omega* **2020**, *5*, 3924–3931. [CrossRef]
199. Kaur, N.; Bharti, A.; Batra, S.; Rana, S.; Rana, S.; Bhalla, A.; Prabhakar, N. An electrochemical aptasensor based on graphene doped chitosan nanocomposites for determination of Ochratoxin A. *Microchem. J.* **2019**, *144*, 102–109. [CrossRef]
200. Wang, Y.; Zhao, G.; Zhang, G.; Zhang, Y.; Wang, H.; Cao, W.; Li, T.; Wei, Q. An electrochemical aptasensor based on gold-modified MoS_2/rGO nanocomposite and gold-palladium-modified Fe-MOFs for sensitive detection of lead ions. *Sens. Actuators B Chem.* **2020**, *319*, 128313. [CrossRef]
201. Qin, B.; Yang, K. Voltammetric aptasensor for thrombin by using a gold microelectrode modified with graphene oxide decorated with silver nanoparticles. *Microchim. Acta* **2018**, *185*, 407. [CrossRef]
202. Li, Y.; Wang, Q.; Zhang, Y.; Deng, D.; He, H.; Luo, L.; Wang, Z. A label-free electrochemical aptasensor based on graphene oxide/double-stranded DNA nanocomposite. *Colloids Surf. B* **2016**, *145*, 160–166. [CrossRef]
203. Li, L.; Yuan, Y.; Chen, Y.; Zhang, P.; Bai, Y.; Bai, L. Aptamer based voltammetric biosensor for *Mycobacterium tuberculosis* antigen ESAT-6 using a nanohybrid material composed of reduced graphene oxide and a metal-organic framework. *Microchim. Acta* **2018**, *185*, 379. [CrossRef]
204. Mazloum-Ardakani, M.; Tavakolian-Ardakani, Z.; Sahraei, N.; Moshtaghioun, S.M. Fabrication of an ultrasensitive and selective electrochemical aptasensor to detect carcinoembryonic antigen by using a new nanocomposite. *Biosens. Bioelectron.* **2019**, *129*, 1–6. [CrossRef] [PubMed]

205. Khosropour, H.; Rezaei, B.; Rezaei, P.; Ensafi, A.A. Ultrasensitive voltammetric and impedimetric aptasensor for diazinon pesticide detection by VS_2 quantum dots-graphene nanoplatelets/ carboxylated multiwalled carbon nanotubes as a new group nanocomposite for signal enrichment. *Anal. Chem. Acta* **2020**, *1111*, 92–102. [CrossRef] [PubMed]
206. Azadbakht, A.; Derikvandi, Z. Aptamer-based sensor for diclofenac quantification using carbon nanotubes and graphene oxide decorated with magnetic nanomaterials. *J. Iran. Chem. Soc.* **2018**, *15*, 595–606. [CrossRef]
207. Bahrami, S.; Abbasi, A.R.; Roushani, M.; Derikvand, Z.; Azadbakht, A. An electrochemical dopamine aptasensor incorporating silver nanoparticle, functionalized carbon nanotubes and graphene oxide for signal amplification. *Talanta* **2016**, *159*, 307–316. [CrossRef]
208. Arvand, M.; Gholami, J. A label-free electrochemical aptasensor for sensitive edifenphos detection in rice. *Anal. Methods* **2020**, *12*, 1237–1243. [CrossRef]
209. Heydari-Bafrooei, E.; Askari, S. Ultrasensitive aptasensing of lysozyme by exploiting the synergistic effect of gold nanoparticle-modified reduced graphene oxide and MWCNTs in a chitosan matrix. *Microchim. Acta* **2017**, *184*, 3405–3413. [CrossRef]
210. El-Wekil, M.M.; Darweesh, M.; Shaykoond MSh, A.; Ali, R. Enzyme-free and label-free strategy for electrochemical oxaliplatin aptasensing by using rGO/MWCNTs loaded with AuPd nanoparticles as signal probes and electro-catalytic enhancers. *Talanta* **2020**, *217*, 121084. [CrossRef]
211. Heydari-Bafrooei, E.; Shamszadeh, N.S. Electrochemical bioassay development for ultrasensitive aptasensing of prostate specific antigen. *Biosens. Bioelectron.* **2017**, *91*, 284–292. [CrossRef]
212. Jia, F.; Duan, N.; Wu, S.; Dai, R.; Wang, Z.; Li, X. Impedimetric *Salmonella* aptasensor using a glassy carbon electrode modified with an electrodeposited composite consisting of reduced graphene oxide and carbon nanotubes. *Microchim. Acta* **2016**, *183*, 337–344. [CrossRef]
213. Appaturi, J.N.; Pulingam, T.; Thong, K.L.; Muniandy, S.; Ahmad, N.; Leo, B.F. Rapid and sensitive detection of Salmonella with reduced graphene oxide-carbon nanotube based electrochemical aptasensor. *Anal. Biochem.* **2020**, *589*, 113489. [CrossRef]
214. Song, J.; Huang, M.; Jiang, N.; Zheng, S.; Mu, T.; Meng, L.; Liu, Y.; Liu, J.; Chen, G. Ultrasensitive detection of amoxicillin by TiO_2-g-C_3N_4@AuNPs impedimetric aptasensor: Fabrication, optimization, and mechanism. *J. Hazard. Mater.* **2020**, *391*, 122024. [CrossRef] [PubMed]
215. Wang, X.; Gao, W.; Yan, W.; Li, P.; Zou, H.; Wei, Z.; Guan, W.; Ma, Y.; Wu, S.; Yu, Y.; et al. A Novel aptasensor based on graphene/graphite carbon nitride nanocomposites for cadmium detection with high selectivity and sensitivity. *ACS Appl. Nano Mater.* **2018**, *1*, 2341–2346. [CrossRef]
216. Duan, F.; Zhang, S.; Yang, L.; Zhang, Z.; He, L.; Wang, M. Bifunctional aptasensor based on novel two-dimensional nanocomposite of MoS_2 quantum dots and g-C_3N_4 nanosheets decorated with chitosan-stabilized Au nanoparticles for selectively detecting prostate specific antigen. *Anal. Chim. Acta* **2018**, *1036*, 121–132. [CrossRef] [PubMed]
217. Xu, H.; Zhang, T.; Gu, Y.; Yan, X.; Lu, N.; Liu, H.; Xu, Z.; Xing, Y.; Song, Y.; Zhang, Z.; et al. An electrochemical thrombin aptasensor based on the use of graphite-like C3N4 modified with silver nanoparticles. *Microchim. Acta* **2020**, *187*, 163. [CrossRef] [PubMed]
218. Jalalvand, A.R. Fabrication of a novel and ultrasensitive label-free electrochemical aptasensor for detection of biomarker prostate specific antigen. *Intern. J. Biol. Macromol.* **2019**, *126*, 1065–1073. [CrossRef] [PubMed]
219. You, H.; Mu, Z.; Zhao, M.; Zhou, J.; Chen, Y.; Bai, L. Voltammetric aptasensor for sulfadimethoxine using a nanohybrid composed of multifunctional fullerene, reduced graphene oxide and Pt@Au nanoparticles, and based on direct electron transfer to the active site of glucose oxidase. *Microchim. Acta* **2019**, *186*, 1. [CrossRef] [PubMed]
220. Roushani, M.; Shahdost-fard, F.; Azadbakht, A. Using Au@nano-C_{60} nanocomposite as an enhanced sensing platform in modeling a TNT aptasensor. *Anal. Biochem.* **2017**, *534*, 78–85. [CrossRef]
221. Chen, Y.; Liu, X.; Guo, S.; Cao, J.; Zhou, J.; Zuo, J.; Bai, L. A sandwich-type electrochemical aptasensor for *Mycobacterium tuberculosis* MPT64 antigen detection using C_{60} NPs decorated N-CNTs/GO nanocomposite coupled with conductive PEI-functionalized metal-organic framework. *Biomaterials* **2019**, *216*, 119253. [CrossRef]
222. Bai, L.; Chen, Y.; Bai, Y.; Chen, Y.; Zhou, J.; Huang, A. Fullerene-doped polyaniline as new redox nanoprobe and catalyst in electrochemical aptasensor for ultrasensitive detection of Mycobacterium tuberculosis MPT64 antigen in human serum. *Biomaterials* **2017**, *133*, 11–19. [CrossRef]

223. Yao, J.; Liu, C.; Yang, M. An ultrasensitive and highly selective electrochemical aptasensor for environmental endocrine disrupter bisphenol A determination using gold nanoparticles/nitrogen, sulfur, and phosphorus co-doped carbon dots as signal enhancer and its electrochemical kinetic research. *J. Electrochem. Soc.* **2019**, *166*, B1161–B1170. [CrossRef]
224. Fakude, C.T.; Arotiba, O.A.; Mabuba, N. Electrochemical aptasensing of cadmium (II) on a carbon black-gold nanoplatform. *J. Electroanal. Chem.* **2020**, *858*, 113796. [CrossRef]
225. Jiao, Y.; Hou, W.; Fu, J.; Guo, Y.; Sun, X.; Wang, X.; Zhao, J. A nanostructured electrochemical aptasensor for highly sensitive detection of chlorpyrifos. *Sens. Actuators B Chem.* **2017**, *243*, 1164–1170. [CrossRef]
226. Abazar, F.; Noorbakhsh, A. Chitosan-carbon quantum dots as a new platform for highly sensitive insulin impedimetric aptasensor. *Sens. Actuators B Chem.* **2020**, *304*, 127281. [CrossRef]
227. Hu, M.; Li, Z.; Guo, X.; Wang, M.; He, L.; Zhang, Z. Hollow core-shell nanostructured MnO_2/Fe_2O_3 embedded within amorphous carbon nanocomposite as sensitive bioplatform for detecting protein tyrosine kinase-7. *Appl. Surf. Sci.* **2019**, *489*, 13–24. [CrossRef]
228. Wang, M.; Hu, B.; Yang, C.; Zhang, Z.; He, L.; Fang, S.; Qu, X.; Zhang, Q. Electrochemical biosensing based on protein-directed carbon nanospheres embedded with SnO_x and TiO_2 nanocrystals for sensitive detection of tobramycin. *Biosens. Bioelectron.* **2018**, *99*, 176–185. [CrossRef] [PubMed]
229. Suib, S.L. A Review of recent developments of mesoporous materials. *Chem. Rec.* **2017**, *17*, 1169–1183. [CrossRef] [PubMed]